Heliyon 10 (2024) e32258

Contents lists available at ScienceDirect

Heliyon

journal homepage: www.cell.com/heliyon

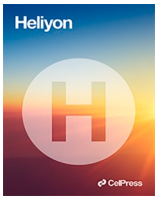

Research article

Prognostic and therapeutic model based on disulfidptosis-related genes for patients with clear cell renal cell carcinoma

Shiyong Xin [a,*], Junjie Su [a], Ruixin Li [a], Qiong Cao [b], Haojie Wang [c], Zhihao Wei [d], Chengliang Wang [e], Chengdong Zhang [f], Jianguo Zhang [a], Zheng Zhang [a], Guanyu Li [a], Wang Qin [a]

[a] *Department of Urology, The First Affiliated Hospital and College of Clinical Medicine of Henan University of Science and Technology, Luoyang, 471000, China*
[b] *Department of Pathology, The Third Affiliated Hospital of Henan University of Science and Technology, 471003, China*
[c] *Department of Central Laboratory, Zhengzhou University, Luoyang Central Hospital, Luoyang, 471003, China*
[d] *Department of Pathology, The Yiluo Hospital of Luoyang, The Teaching Hospital of Henan University of Science and Technology, Luoyang, 471023, China*
[e] *Department of Urology, Shangcheng County People's Hospital, Xinyang, 464000, China*
[f] *Department of Urology, Xinxiang City First People's Hospital, Xinxiang, 453000, China*

ARTICLE INFO

Keywords:
Disulfidptosis
Clear cell renal cell carcinoma
Prognosis
Immune cell infiltration

ABSTRACT

Disulfidptosis, a newly discovered mode of cell death caused by excessive accumulation of intracellular disulfide compounds, is closely associated with tumor development. This study focused on the relationship between disulfidptosis and clear cell renal cell carcinoma (ccRCC). Firstly, the characterizations of disulfidptosis-related genes (DRGs) in ccRCC were showed, which included number variation (CNV), single nucleotide variation (SNV), DNA methylation, mRNA expression and gene mutation. Then, the ccRCC samples were classified into three clusters through unsupervised clustering based on DRGs. Survival and pathway enrichment differences were evaluated among the three clusters. Subsequently, the differentially expressed genes (DEGs) among the three clusters were screened by univariate Cox, LASSO, and multivariate Cox analysis, and five key DEGs were obtained. Based on the five key DEGs, the ccRCC samples were reclassified into two geneclusters and the survival differences and immune cell infiltration between two geneclusters was investigated. In next step, ccRCC samples were divided into two groups according to PCA scores of five key DEGs, namely high PCA score group (HPSG) and low PCA score group (LPSG). On this basis, differences in survival prognosis, immune cell infiltration and correlation with immune checkpoint, as well as differences in sensitivity to targeted drugs were compared between HPSG and LPSG. The expression levels of four immune checkpoints were higher in HPSG than in LPSG, whereas the LPSG was more sensitive to targeted drug therapy than the HPSG. Finally, validation experiments on HDAC4 indicated that HDAC4 could increase the proliferation and colony formation ability of ccRCC cells.

* Corresponding author. Department of Urology, The First Affiliated Hospital and College of Clinical Medicine of Henan University of Science and Technology, No. 636, Guan-lin Rd, Luo-long District, Luoyang, China.
E-mail address: doctsyxin@163.com (S. Xin).

https://doi.org/10.1016/j.heliyon.2024.e32258
Received 30 December 2023; Received in revised form 30 May 2024; Accepted 30 May 2024
Available online 2 June 2024

1. Introduction

Renal cell carcinoma (RCC) is the most common kidney malignant tumor in adults, and its incidence has gradually been increasing in the recent years. Of all RCC subtypes, clear cell renal cell carcinoma (ccRCC) is the most common subtype, accounting for approximately 75 % of all cases [1,2]. However, because of the lack of early typical symptoms in patients with ccRCC and a high degree of clinical heterogeneity, approximately 25 %–30 % of patients have already developed metastases at diagnosis [3]. In addition, for advanced or metastatic ccRCC patients, there are no effective treatment strategies currently available [4]. Therefore, given the high incidence and mortality rates of ccRCC, it is particularly important to develop new and effective treatment strategies.

List of abbreviations

ccRCC	Clear cell renal cell carcinoma
HPSG	High PCA score group
LPSG	Low PCA score group
DRGs	Disulfidptosis-related genes
RCC	Renal cell carcinoma
DEG	Differentially expressed gene
SLC7A11	Solute carrier family 7 member 11
CRISPR	Clustered regularly interspaced short palindromic repeats
SLC3A2	Solute carrier family 3 member 2
NCKAP1	NCK associated protein 1
GYS1	Glycogen synthase 1
NDUFS1	NADH:ubiquinone oxidoreductase core subunit S1
NDUFA11	NADH:ubiquinone oxidoreductase subunit A11
OXSM	Mitochondrial 3-oxoacyl-ACP synthase
LRPPRC	Leucine rich pentatricopeptide repeat containing
EMT	Epithelial-mesenchymal transition
EDU	5-ethynyl-2′-deoxyuridine
CNV	Copy-number variation
SNV	Single nucleotide variation
TCGA	The Cancer Genome Atlas Program
GSVA	Gene Set Variation Analysis
KEGG	Kyoto Encyclopedia of Genes and Genomes
TIME	Tumor immune microenvironment
ESTIMATE	Estimation of STromal and Immune cells in Malignant Tumor using Expression data
TIDE	Tumor Immune Dysfunction and Exclusion
CAF	Cancer-Associated Fibroblast
TAM	Tumor-associated macrophage
HPA	Human Protein Atlas
PCA	Principal component analysis
IHC	Immunohistochemistry
qRT-PCR	Quantitative Real-Time Polymerase Chain Reaction
TME	Tumor mircroenviroment
TNBC	Triple-negative breast cancer
HDAC4	Histone deacetylase 4
HK2P1	Hexokinase 2 pseudogene 1
ZNF175	Zinc finger protein 175
CHTF8	Chromosome transmission fidelity factor 8
Treg	Regulatory T
GDSC	Genomics of Drug Sensitivity in Cancer
GSEA	Gene Set Enrichment Analysis

Programmed cell death, including ferroptosis, pyroptosis, and copper-mediated cell death, plays a key role in the human body and has been extensively studied in relation to tumor progression [5,6]. Iron-dependent cell death, also known as ferroptosis, is apoptosis caused by excessive accumulation of intracellular iron-dependent peroxides [7]. It is involved in the progression of pancreatic, bladder, and bowel cancers [8]. In addition, copper-mediated cell death-related genes were shown to be potentially linked to ccRCC development [9]. Recently, Liu et al. discovered a novel cell death pathway, which they named disulfidptosis [10]. Disulfidptosis differs from the currently known cell death mechanisms and is primarily associated with the actin cytoskeleton, which interferes with

its organization, ultimately leading to the collapse of the actin network and cell death [10]. Liu et al. found that under glucose starvation, abnormal accumulation of intracellular disulfide in high Solute carrier family 7 member 11 (SLC7A11high) cells induced a previously uncharacterized form of cell death distinct from apoptosis and iron apoptosis [10]. We call this cell death disulfidptosis. Previous analyses have shown that glucose starvation in SLC7A11high cells induced abnormal disulfide bonds in the actin skeleton protein and f-actin collapse in a SLC7A11-dependent manner. Clustered regularly interspaced short palindromic repeats (CRISPR) screening and functional studies have shown that inactivation of the WAVE regulatory complex (which promotes actin polymerization and plate foot formation) inhibits disulfidptosis, whereas constitutive activation of Rac promotes disulfidptosis. Further research showed that the glucose transporter inhibitors induced double vulcanization of SLC7A11high cancer cells and inhibited the growth of SLC7A11high tumors [10]. The sensitivity of the actin cytoskeleton to disulfide stress-mediated disulfidptosis and a therapeutic strategy for targeting disulfidptosis in cancer therapy were suggested by these findings. Therefore, disulfidptosis may play an indispensable role in tumor progression, and the function of disulfidptosis in ccRCC is worth exploring.

In addition to SLC7A11, solute carrier family 3 member 2 (SLC3A2), and ribophorin I (RPN1), and NCK associated protein 1 (NCKAP1) also contributes greatly to the process of disulfidptosis, and interference with these genes can effectively inhibit the progression of disulfidptosis. Further studies have shown that glycogen synthase 1 (GYS1) can induce disulfidptosis in coordination with mitochondrial oxidative phosphorylation-related genes [NADH:ubiquinone oxidoreductase core subunit S1 (NDUFS1), NADH:ubiquinone oxidoreductase subunit A11 (NDUFA11), mitochondrial 3-oxoacyl-ACP synthase (OXSM), NUBPL, and leucine rich pentatricopeptide repeat containing (LRPPRC)] [10]. As an important regulatory gene of disulfidptosis, SLC7A11 belongs to the cystine/glutamate transporter family and plays a crucial role in transporting cysteine to cells for glutathione biosynthesis and antioxidative defense [11]. SLC7A11 is not only involved in disulfidptosis but is also highly expressed in various solid tumors, such as breast cancer [12] and liver cancer [13]. It also affects the occurrence and development of tumor cells and the treatment and prognosis of patients. In addition, SLC3A2, RPN1, and NCKAP1 play a role in the process of cellular disulfidptosis, and the progression of disulfidptosis can be effectively inhibited by interfering with these genes [10]. SLC3A2 is closely associated with various tumors and highly expressed in various histological types of renal carcinoma, among which ccRCC, papillary carcinoma, and chromophobe cell carcinoma are the most significant [14]. Meanwhile, silencing SLC3A2 can disable the proliferation and metastasis of tumor cells [15]. RPN1 is a part of the N-oligosaccharyl-transferase complex and plays a crucial role in the development of various cancers. The expression of RPN1 in breast cancer tissues is higher than that in normal tissues, and RPN1 can promote the proliferation and migration of tumor cells by activating the PI3K/AKT/mTOR signaling pathway [16]. NCKAP1 is an NCK-related protein gene and a member of the tyrosine kinase-binding protein family. In breast cancer, the expression level of NCKAP1 is negatively associated with the prognosis of patients, and down-regulation of NCKAP1 can inhibit the migration and invasion ability of cancer cells [17]. GYS1 is highly expressed in ccRCC tissue and promotes tumor cell proliferation, making it a potential therapeutic target for ccRCC patients [18]. NDUFS1 can also be used as a diagnostic marker for renal carcinoma, and is also significantly correlated with the pathological stage and grade of renal carcinoma and patient survival; the lower the expression of NDUFS1, the higher the stage and the sooner the occurrence of distant metastasis in a cancer patient [19]. Increased expression of NDUFA11 in breast cancer promotes tumor cell invasion and metastasis by enhancing mitochondrial electron leakage [20]. NUBPL is an assembly factor in human mitochondrial complex I. The mRNA level of NUBPL is significantly elevated in colorectal cancer tissues, and NUBPL enhances the migration and invasive ability of tumor cells by promoting epithelial-mesenchymal transition (EMT) [21]. The LRPPRC is a member of the pentatricopeptide repeat protein family and is located in the cytoplasm and mitochondria. The expression of this sequence is increased in various cancer tissues such as prostate cancer, gastric cancer, and urothelial carcinoma of the bladder and is negatively correlated with patient prognosis [22–24]. OXSM plays a role in colorectal cancer progression, and the risk model constructed by OXSM has the potential to predict survival and prognosis of colorectal cancer patients [25]. These DRGs are closely involved in disulfidptosis, which plays an important role in tumor progression. However, so far, few studies on disulfidptosis have been found in RCC, and the role and mechanism of disulfidptosis in the progression of RCC are unclear. Therefore, it is of great significance to investigate the role of disulfidptosis and its related genes in the occurrence and development of RCC.

In our study, the roles of DRGs in ccRCC were investigated using multi-omics analysis with the aim of establishing a valuable model that can guide the prognosis and treatment of ccRCC. First, we studied mRNA changes of DRGs in tumor samples and normal samples, as well as the DRG mutations in tumor samples. The ccRCC samples were divided into three clusters through unsupervised clustering. Further analysis was conducted to identify key differentially expressed genes (DEGs) by performing univariate, LASSO, and multivariate analysis on DEGs among the three clusters. Based on the key DEGs during screening, ccRCC samples were categorized into two geneclusters by unsupervised clustering. Principal component analysis (PCA) was then performed in the two geneclusters and PCA scores were calculated for each sample. Based on PCA scores, the ccRCC samples were divided into high PCA score group (HPSG) and low PCA score group (LPSG). Survival analysis showed noteworthy differences in survival duration between HPSG and LPSG. Furthermore, a correlation between PCA scores and immune cell infiltration was also identified. Subsequently, the expression characteristics of common immune checkpoints between the two groups were analyzed, and the differences in drug sensitivity and clinical features were determined. Finally, we investigated and confirmed the function of HDAC4 in ccRCC through immunohistochemistry (IHC), Western blotting, colony formation, and 5-ethynyl-2′-deoxyuridine (EDU).

2. Materials and methods

2.1. Data collection

Data used in our study including transcriptomic, clinical, copy number variation (CNV), single nucleotide variation (SNV), and

DNA methylation data of 541 ccRCC samples and 72 normal samples were download from The Cancer Genome Atlas Program (TCGA) database on March 5, 2023. Of these, 11 poor quality ccRCC samples with a survival time of 0 were removed, leaving 530 ccRCC samples for subsequent analyses. In addition, 10 DRGs including GYS1, RPN1, SLC7A11, NDUFA11, NCKAP1, LRPPRC, OXSM, SLC3A2, NUBPL, and NDUFS1 were obtained from the published literature [10]. Further, SNV, CNV, DNA methylation, mutation, and mRNA expression of 10 DRGs was performed by R in ccRCC. 15 pairs of fresh ccRCC tissue (cancer and adjacent normal tissue) and paraffin sections from 30 cases of ccRCC patients were collected for IHC. All experimental procedures were approved by the Ethics Committee of First Affiliated Hospital of Henan University of Science and Technology.

2.2. Differential analysis of DRGs

First, we standardized and normalized ccRCC and normal samples from the TCGA database using the Limma package [26]. Next, the mRNA expression matrices of the 10 DRGs were extracted and the 10 DRGs were differentially analyzed in tumor and normal samples following the unpaired *t*-test method (student t-test).

2.3. Cluster analysis of the ten DRGs

Based on the mRNA expression levels of the 10 DRGs, 530 ccRCC samples were classified into three clusters, cluster 1, cluster 2, and cluster 3 by unsupervised clustering using the ConsensusClusterPlus package (version: 4.22) [27]. Kaplan-Meier survival analysis (log-rank test) was used to analyze the differences in survival time of samples among the three clusters, with $p < 0.05$ as the significance threshold.

2.4. Functional differences and DEGs among the three clusters

Based on the mRNA expression matrix obtained from the abovementioned normalization, the three clusters obtained in the previous step were differentially analyzed using the Limma package. A significance threshold of $|\log2FoldChange\ (FC)| > 0$ and FDR <0.05 was used to determine statistical significance. Differential results were visualized using volcano plots and Venn diagrams. In addition, enrichment pathways differences among the three clusters were analyzed by Gene Set Variation Analysis (GSVA) [28] based on Hallmarks of Cancer [29] and the Kyoto Encyclopedia of Genes and Genomes (KEGG), which were visualized by heatmap.

2.5. Identification of key DEGs and their prognostic analysis

First, univariate Cox analysis was performed for screening DEGs. Then, to solve collinearity and overfitting problems, LASSO analysis was performed using "glmnet" package (Version 4.22) to further filter prognostic DEGs. Finally, based on the results of LASSO algorithm, five key DEGs were selected by multivariate Cox regression analysis. The prognostic value of five key DEGs was investigated by Kaplan-Meier survival analysis.

2.6. Cluster analysis of the five key DEGs

Based on the mRNA expression data of the five DEGs, the ccRCC samples were divided into two geneclusters, namely genecluster A and genecluster B, by unsupervised clustering using the ConsensusClusterPlus package. The two geneclusters expression matrices obtained in the previous step were used for pathway enrichment analysis based on the Hallmarks of Cancer and KEGG using the R package GSVA.

2.7. Differences in the tumor immune microenvironment (TIME)

Differences in the abundance of 22 immune cell infiltrations between the two geneclusters were investigated by CIBERSORT, relying on gene expression data. In addition, to evaluate the heterogeneity of the TIME, we computed tumor stromal cell infiltration, immune cell infiltration, and tumor purity using the Estimation of STromal and Immune cells in Malignant Tumor using Expression data (ESTIMATE) method [30]. Gene expression data of the ccRCC samples were uploaded to the Tumor Immune Dysfunction and Exclusion (TIDE) website (http://tide.dfci) [31], and the Cancer-Associated Fibroblast (CAF) score, Tumor-Associated Macrophage M2 (TAM M2) score, TIDE score, and Exclusion score were calculated for each of the two geneclusters. The differences were then visualized using box plots.

2.8. PCA score model construction

First, the distribution of the samples in the two geneclusters was analyzed and presented by PCA. The PCA score was obtained by calculating the sum of PC1 and PC2 for each sample, and ccRCC samples were then divided into HPSG and LPSG based on the PCA score. Survival differences between the HPSG and LPSG were analyzed using Kaplan-Meier survival analysis. Further differences in abundance of immune cell infiltration and expression of four immune checkpoints were analyzed between HPSG and LPSG using the ggplot2 package. The relationship between DRGs, key DEGs, and PCA score in ccRCC samples was analyzed using the R package ggcor.

2.9. Clinical characteristics

The clinical characteristics data of 530 ccRCC patients downloaded from the TCGA database. The downloaded clinical data were used to analyze the differences in age, survival status, stage grade and T stage between HPSG and LPSG patients by the ggplot2 and ggpubr packages.

2.10. Drug screening

First, we downloaded the expression data of cell lines and data of the drug sensitivities of cell lines to 283 drugs from Genomics of Drug Sensitivity in Cancer (GDSC) (https://www.cancerrxgene.org/). Subsequently, we used the Oncopredict package [32] to perform drug sensitivity analyses and ascertain the IC50 values of drugs in the HPSG and LPSG. This analysis aimed to assess differences in drug treatment sensitivity between HPSG and LPSG.

2.11. The human protein atlas (HPA)

The HPA (https://www.proteinatlas.org/) [33] is a comprehensive resource based on multi-omics data that includes tissue, cell, and organ atlases covering both cancerous and normal tissues. Corresponding immunohistochemical sections were retrieved from the database and analyzed for differences in HDAC4 and ZNF175 protein levels between tumor and normal samples.

2.12. Relationship of Wnt and EMT gene sets with key DEGs

We downloaded the related gene data for Wnt and EMT pathway from the official Gene Set Enrichment Analysis (GSEA) website [GSEA | MSigDB (gsea-msigdb.org)] and the dbEMT 2.0 website, respectively. Further, we calculated the Wnt and EMT pathway score for each sample using GSEA, and then performed correlation analysis between the expression of five key DEGs and the pathway score.

2.13. IHC

The clinical tissue sections (Tumor:Normal = 30:30) were collected for immunohistochemical staining. The collected paraffin sections were first dewaxed. Sections were hydrated by passing through an alcohol of gradient concentration. Sections were then heated in antigen repair solution and further treated with 3 % hydrogen peroxide and PBS, respectively. After drying, a primary antibody (Proteintech 17449-1-AP, 1:100) was added and incubated at 4° overnight. The next day, the secondary antibody was added and the sections were washed with PBS after 1 h. Subsequently, DAB chromogen was added and staining was stopped after observing that the cells were appropriately stained, followed by rinsing with water. Finally, the sections were stained with hematoxylin. The IHC results were scored by two experienced pathologists. The intensity of cell staining: no staining (negative) was 0 point, light yellow (weak positive) was 1 point, brown yellow (positive) was 2 points, tan (strong positive) was 3 points; According to the percentage of positive cells, 1 point for $\leq$25 %, 2 points for 26%–50 %, 3 points for 51%–75 %, and 4 points for $\geq$75 %. The two scores were multiplied to yield the final score. The two scores were multiplied to give the final results.

2.14. Cell treatment

Cell lines (786-O) were obtained from HyCyteTM (TCH-C107, Hai xing, China). Si-HDAC4 was designed and synthesized by GenePharma Co., Ltd. (Shanghai, China). The 786-O cells were seeded in six-well plates before transfection. When the observed cell density reached approximately 80 %, transfection was performed using Lipofectamine 3000 (Invitrogen, Carlsbad, USA), according to the manufacturer's instructions.

2.15. RNA extraction and quantitative real-time polymerase chain reaction (qRT-PCR)

To quantify HDAC4 mRNA levels, RNA was first extracted from cells using a TRIzol reagent (TaKaRa, China). The cDNA was obtained by reverse transcription using a reverse HiFiScript cDNA synthesis kit (CWBio, China). Subsequently, qPCR was performed on StepOne (Thermo, China) using SYBR Green qPCR Kit (TaKaRa, China). Three replicates were performed for each experiment, and the expression of HDAC4 was detected following the $2^{-\Delta\Delta Ct}$ method. The primer sequence was as follows: forward 5′-GGCCCACCG-GAATCTGAAC-3′; reverse 5′-GAACTCTGGTCAAGGGAACTG-3′.

2.16. Western blotting

Cell Western blotting: Cells were treated with RIPA lysis buffer (Solarbio). The extracted proteins were separated on SDS-PAGE gels (12 %, Beyotime) and transferred to polyvinylidene fluoride membranes (PVDF, Millipore). After blocking with skimmed milk powder, primary antibody (Cell Signaling Technology, 7628T, 1:1500) was added and the cells were incubated overnight at 4 °C. The following day, the primary antibody was washed off and the secondary antibody was added. The cells were then incubated for 2 h.

Tissue Western blotting (15 pairs of fresh cancer and adjacent normal tissue): First, the tissue was cut into pieces on ice; the tissue fragments were transferred to a glass homogenizer and cold PBS was added in a 1:5 ratio for grinding a homogenate. The homogenate

was centrifuged at 5000 *g* for 5 min, and the supernatant was collected for detection. The subsequent steps were the same as those followed for cell Western blotting.

2.17. Cell proliferation and colony formation

The proliferative capacity of cells was determined using the BeyoClickTM EDU-555 Cell Proliferation Assay Kit (Beyotime). Cells (2×10^5/well) were inoculated into a 6-well plate and when the cells were stable, they were treated according to standard experimental procedures.

The transfected cells (1×10^3/well) were transferred to a 6-well plate and incubated in an incubator for two weeks. The cells were then fixed with 4 % paraformaldehyde and observed after staining with 1 % crystallization.

2.18. Statistics and software

Bioinformatics analysis was performed using R version 4.2.2. Statistical analysis was performed using GraphPad Prism 8 (GraphPad Software, Inc.). Continuous data were compared using student *t*-test or Wilcoxon test. Clinical and pathological parameters were compared by Chi-square test and Fisher test. Kaplan–Meier curve was used to evaluate the survival rate. Independent parameters related to overall survival were analyzed by univariate and multivariate Cox regression analysis using log-rank test. The Pearson correlation coefficient was calculated to measure the correlation between two variables. Regression analysis was performed by the LASSO method. The "glmnet" R package was used to build predictive models. Spearman correlation analysis was used to analyze the

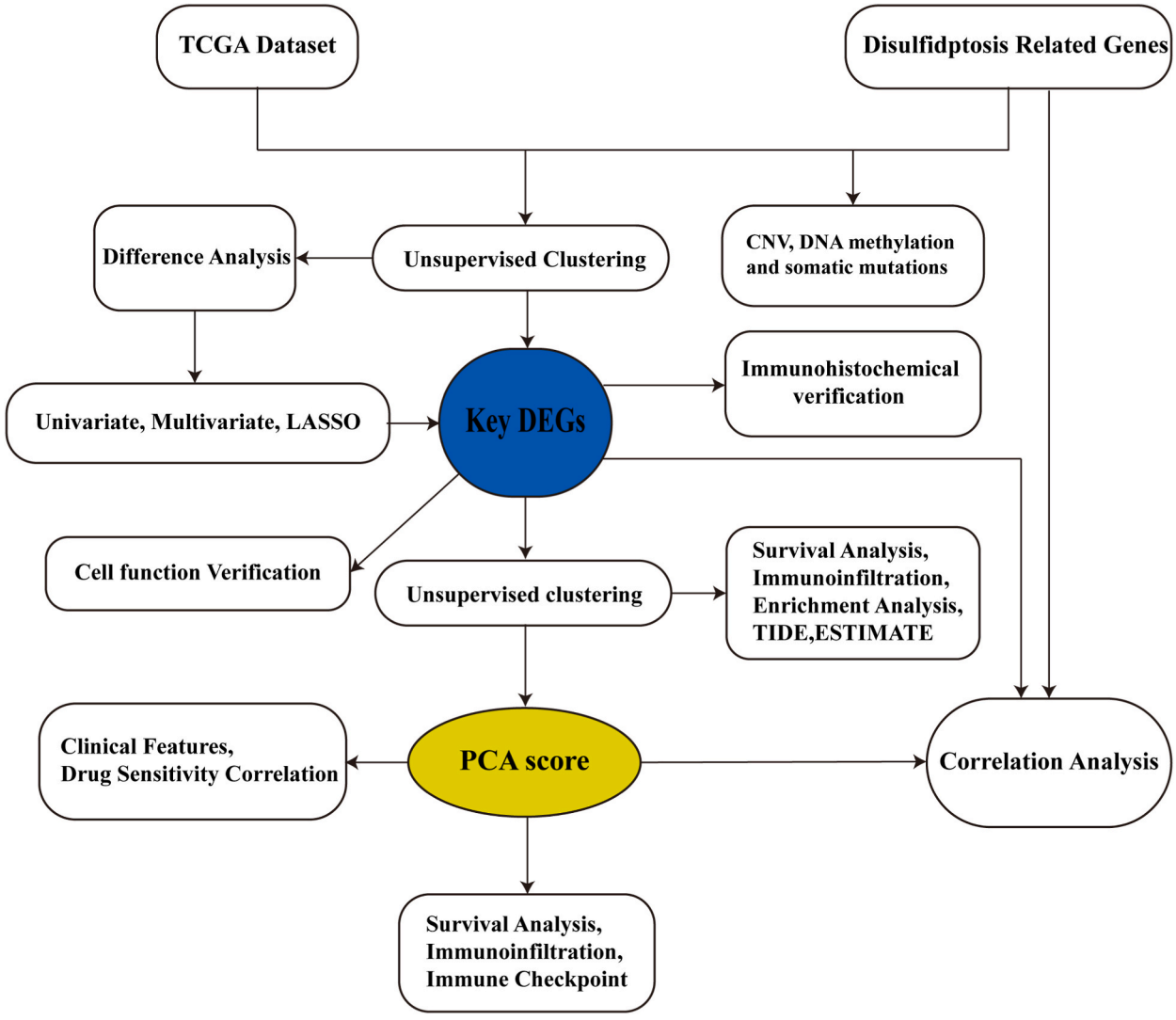

Fig. 1. A flow chart of the research conducted.

correlation. The results of multivariate Cox regression analysis are represented by normal graphs. All p values were bilateral.***p < 0.001, **p < 0.01, *p < 0.05, and nsp >0.05.

3. Results

3.1. Study work flow

In this study, we explored the role of disulfidptosis in ccRCC through bioinformatics analysis of ccRCC data from multiple databases, and conducted related experimental validation aimed at advancing our understanding and knowledge of RCC (Fig. 1).

3.2. Expression and mutation characteristics of DRGs in ccRCC

Based on the data obtained from the TCGA database, the mRNA expression, mutation and methylation of 10 DRGs were investigated and we found that the expression levels of SLC7A11 and GYS1 were significantly increased in ccRCC samples compared with normal renal tissue, whereas the expression levels of NDUFS1, LRPPRC, NCKAP1, NUBPL, OXSM, and SLC3A2 were increased in normal tissue compared with ccRCC tissue (Fig. 2A–B). Through the results shown in the waterfall diagram, we discovered that 14 ccRCC samples had mutations in DRGs, and nonsense mutations were the main ones. NDUFS1 had the highest mutation frequency, with mutations in 5 samples (Fig. 2C). By analyzing the CNV of DRGs, our results showed that copy number loss of OXSM, NUBPL, and SLC7A11 was dominant in ccRCC, whereas copy number amplification of NCKAP1, LRPPRC, and GYS1 was dominant in ccRCC (Fig. 2D). SNV percentage heatmap showed that NDUFS1 had the highest SNV percentage in ccRCC, followed by LRPPRC (Supplementary Fig. 2C). Based on methylation-related results, we found that LRPPRC, OXSM, and NUBPL had higher levels of methylation in ccRCC samples than in normal samples. By combining with the mRNA expression data, the results indicated that the methylation level of NCKAP1 was positively correlated with mRNA expression. However, the methylation levels of NUBPL and NDUFA11 were negatively correlated with mRNA levels (Fig. 2E–F). This suggested that the methylation of NDUFSA led to an increase in its mRNA expression level, whereas the methylation of NUBPL and NDUFA11 inhibited gene transcription, resulting in a decrease in mRNA level.

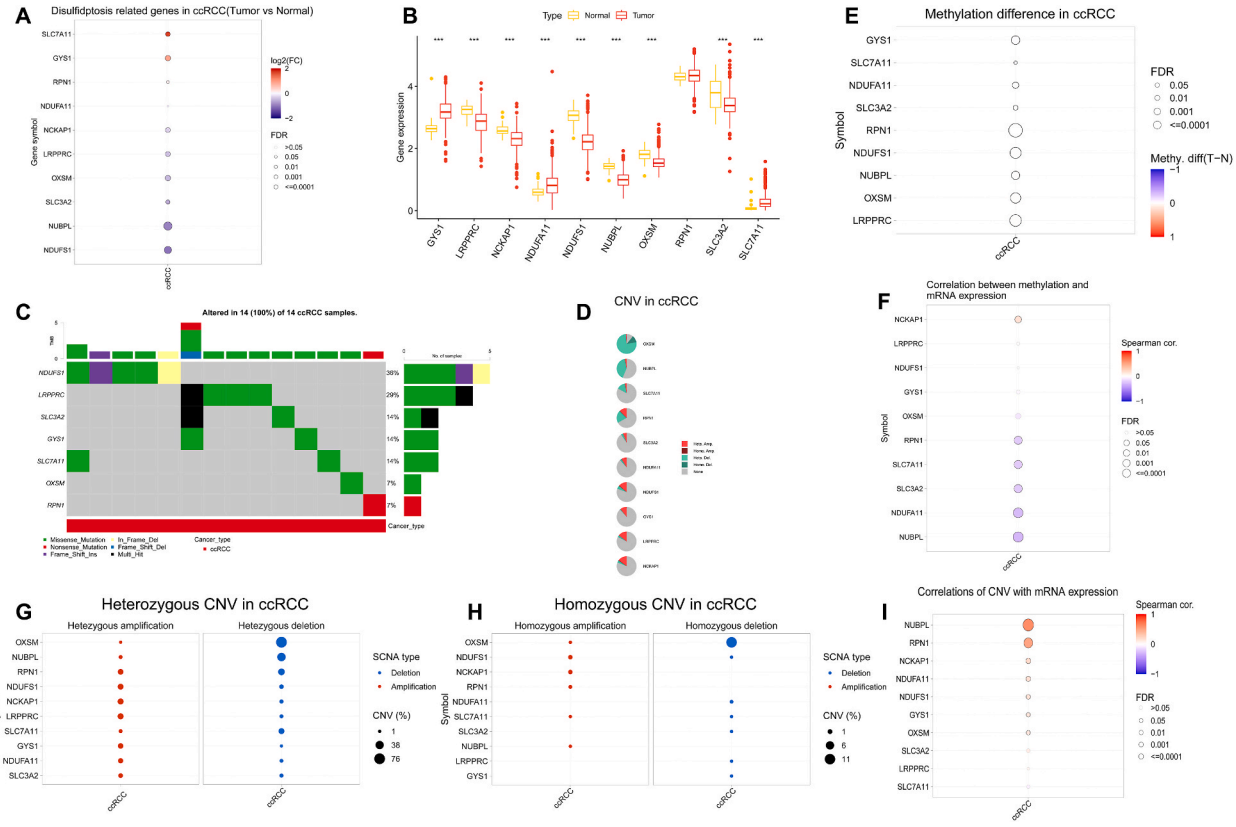

Fig. 2. Differential expression, CNV, DNA methylation, and somatic mutations of 10 DRGs in ccRCC. (A) Differential expression of DRGs in ccRCC. (B) Differential expression of DRGs between normal and tumor tissues. (C) The Waterfall demonstrates the somatic mutation frequency of DRGs in ccRCC. (D) CNV of DRGs in ccRCC. (E) Differential DNA methylation between tumor and normal samples in ccRCC. (F) The correlation between DNA methylation and gene mRNA expression. (G) The figure depicts the heterozygous CNV landscape of genes in ccRCC. (H) The figure illustrates the homozygous CNV landscape of genes in ccRCC. (I) The relationship between CNV and gene expression.

Meanwhile, our results showed that NCKAP1 and LRPPRC had the highest level of copy number heterozygote amplification, and OXSM had the highest level of copy number heterozygote deletion. Among homozygous CNVs, NDUFS1 and NCKAP1 had the highest level of amplification and OXSM had the highest level of deletion (Fig. 2G–H). By analyzing the correlation between CNVs and mRNA expression of 10 DRGs, we found that except for SLC7A11, CNV of the remaining genes was positively correlated with mRNA expression (Fig. 2I).

3.3. ccRCC samples clustering and prognostic analysis and DEG pathway enrichment

In this step, based on mRNA expression levels of 10 DRGs, 530 ccRCC samples were classified into three clusters (cluster 1, cluster 2, and cluster 3) through unsupervised cluster analysis using the ConsensusClusterPlus package (Fig. 3A). Furthermore, survival differences among the three clusters were detected, and the results showed that survival probability in cluster 1 was the lowest among three clusters (Fig. 3B). Furthermore, we found that two (NUBPL and RPN1) among the 10 DRGs correlated with ccRCC patient survival. In particular, the survival probability of patients in low NUBPL expression group was higher than that of patients in high NUBPL expression group, whereas the survival probability of patients in the high RPN1 expression group was higher than that of patients in the low RPN1 expression group (Fig. 3C–D). However, there was no discernible disparity in the survival probability between the high and low expression groups of the remaining eight genes (Supplementary Figs. 1A–H). The volcano plot and Venn diagram were used to illustrate the DEGs among the three clusters and 2693 DEGs were detected (Fig. 4A–D) (Supplementary Tables S1–3). Furthermore, the enrichment analysis results from Hallmark and KEGG revealed significant functional differences among the three clusters. Compared with cluster 2 and cluster 3, cluster 1 was predominantly enriched in several metabolic pathways, such as bile acid

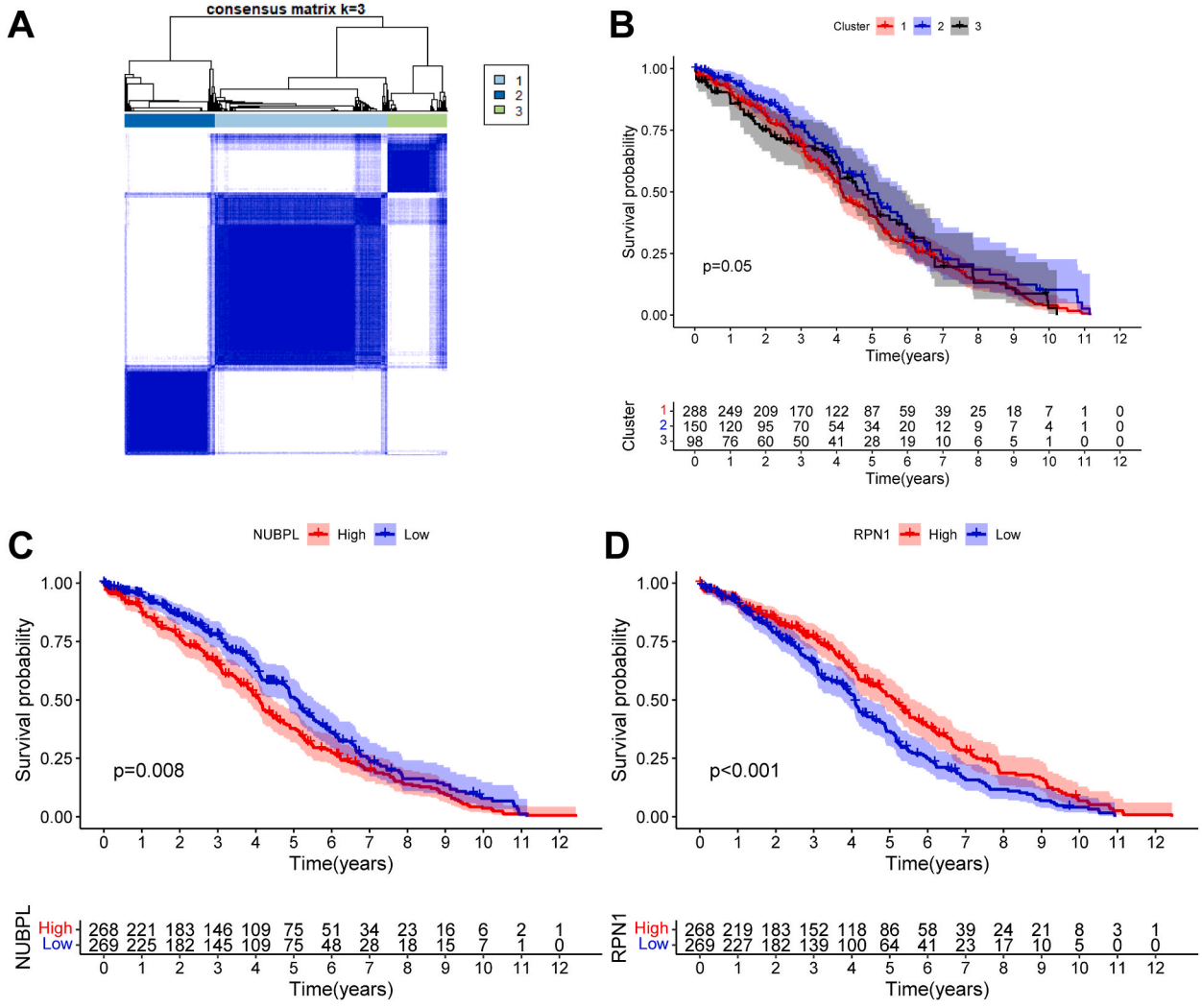

Fig. 3. Unsupervised clustering analysis based on the mRNA expression of DRGs. (A) The samples were divided into three clusters by unsupervised clustering analyses. (B) Kaplan–Meier survival curves of three clusters. (C–D) Kaplan–Meier survival curves of DRGs.

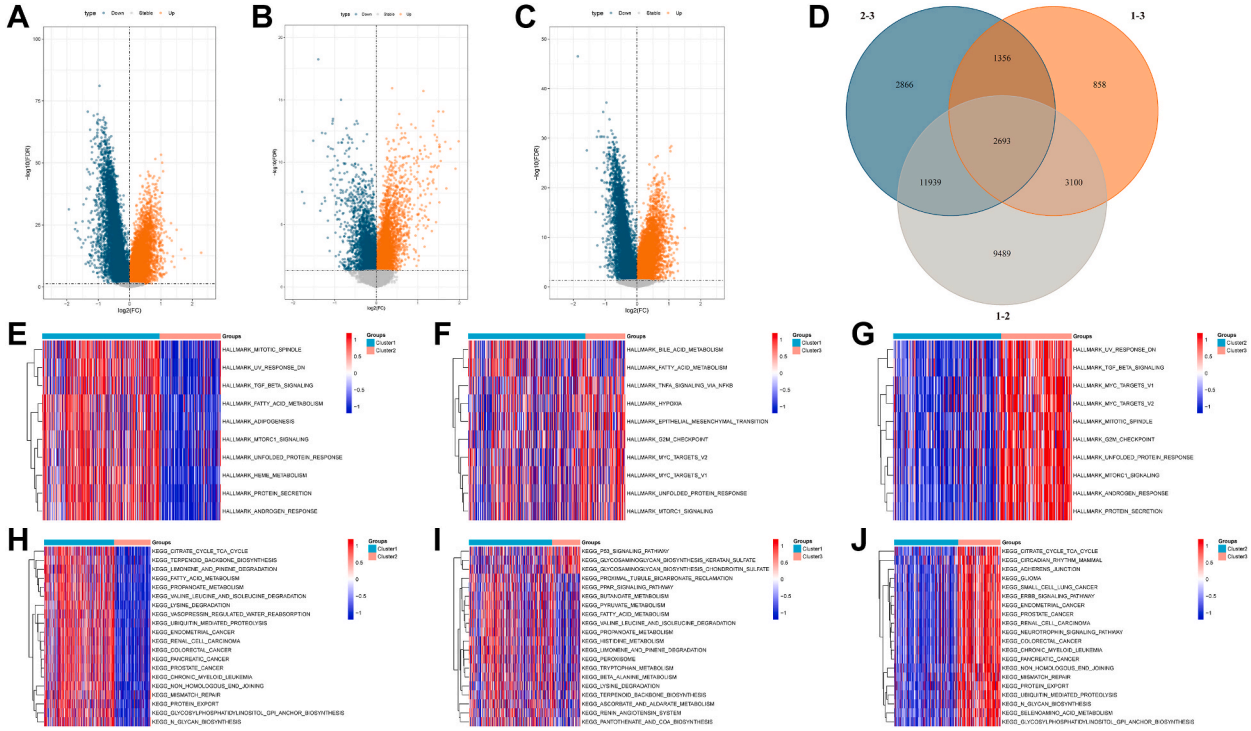

Fig. 4. Differential analysis and GSVA analysis. (A–C) Differential expression gene analysis of the three clusters. (D) Venn diagram illustrating the DEGs. The (E–G) HALLMARK pathway and (H–J) KEGG pathway were downloaded separately from the Msigdb database and the pathways were scored by the R package GSVA.

metabolism, fatty acid metabolism, and various amino acid metabolic pathways. On the other hand, cluster 3 exhibited significant enrichment in pathways such as those associated with myc targets, G2M checkpoint, prostate cancer, and renal cell carcinoma (Fig. 4E–J).

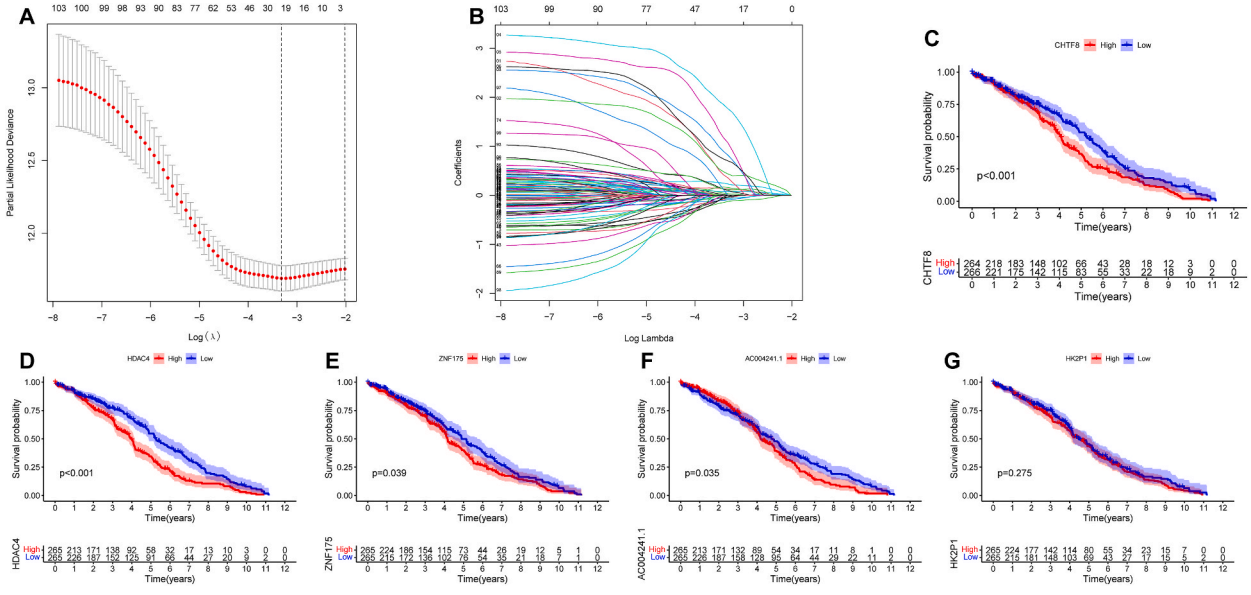

Fig. 5. Screening of the five key DEGs. (A–B) Lasso analysis was performed to screen DEGs. (C–G) Kaplan–Meier survival analysis of low-expression and high-expression groups of CHTF8, HDAC4, ZNF175, AC004241.1, and HK2P1.

3.4. Two geneclusters were established through unsupervised clustering based on five key DEGs

In the previous step, we divided ccRCC samples into 3 clusters based on 10 DRGs, and compared prognostic differences among the 3 clusters, as well as DEGs of 3 clusters and their enrichment analyses. In this step, five key DEGs were screened by LASSO regression, which was conducted with the "glmnet" package in RStudio, univariate (Supplementary Table 4, Supplementary Fig. 2A) and multivariate (Supplementary Table 5, Supplementary Fig. 2B) Cox regression analysis (Fig. 5A–B). Survival analysis on the five key DEGs showed that the survival probability of patients with high expression levels of CHTF8, HDAAC4, ZNF175, and AC004241.1 was significantly lower than that of patients with low expression levels($P < 0.05$) (Fig. 5C–F). However, there was no difference with regard to survival prognosis between high and low HK2P1 groups (Fig. 5G).

In next step, the ccRCC samples were divided into two geneclusters through unsupervised clustering based on the five key DEGs (Fig. 6A). The genecluster A showed higher expression levels of four DEGs (ZNF175, HDAC4, HK2P1, and CHTF8) than the genecluster B ($P < 0.05$) (Fig. 6B). Subsequently, we analyzed the correlation between five key DEGs and EMT and Wnt score. Our results confirmed that AC004241.1, CHTF8, HDAC4, HK2P1, and ZNF175 were positively associated with EMT score; Furthermore, HDAC4 and ZNF175 were positively correlated with Wnt score, whereas AC004241.1 was negatively correlated with Wnt score (Fig. 6C). Among the five key DEGs, HDAC4 had a strong correlation with EMT and Wnt signaling pathways (Fig. 6C). Furthermore, survival analysis was conducted between the two geneclusters, and our results indicated that genecluster B had a higher survival rate than genecluster A (Fig. 6D). The results of KEGG and Hallmark enrichment analyses showed that compared with cluster A, cluster B was mainly enriched in G2M checkpoint, renal cell carcinoma, mismatch repair, and TGF BETA pathways (Fig. 6E–F). Subsequently, the infiltration of 22 immune cells in ccRCC TIME, the differences in TME pattern, and TIDE between two geneclusters were investigated. Using the CIBERSORT algorithm, the infiltration of 22 immune cells was detected between two geneclusters (Supplementary Table 6). Among them, CD8 T cells, activated CD4 memory T cells, T cell follicular helper, and regulatory T (Treg) cells exhibited greater infiltration abundance in genecluster B than genecluster A (Fig. 6G). Meanwhile, the results from the ESTIMATE algorithm indicated that genecluster B had higher ImmuneScore and ESTIMATE Score than genecluster A (Fig. 6H) (Supplementary Table 7); this finding is in accordance with the findings from CIBERSORT analysis. Furthermore, using the TIDE algorithm, we observed higher scores for CAF,

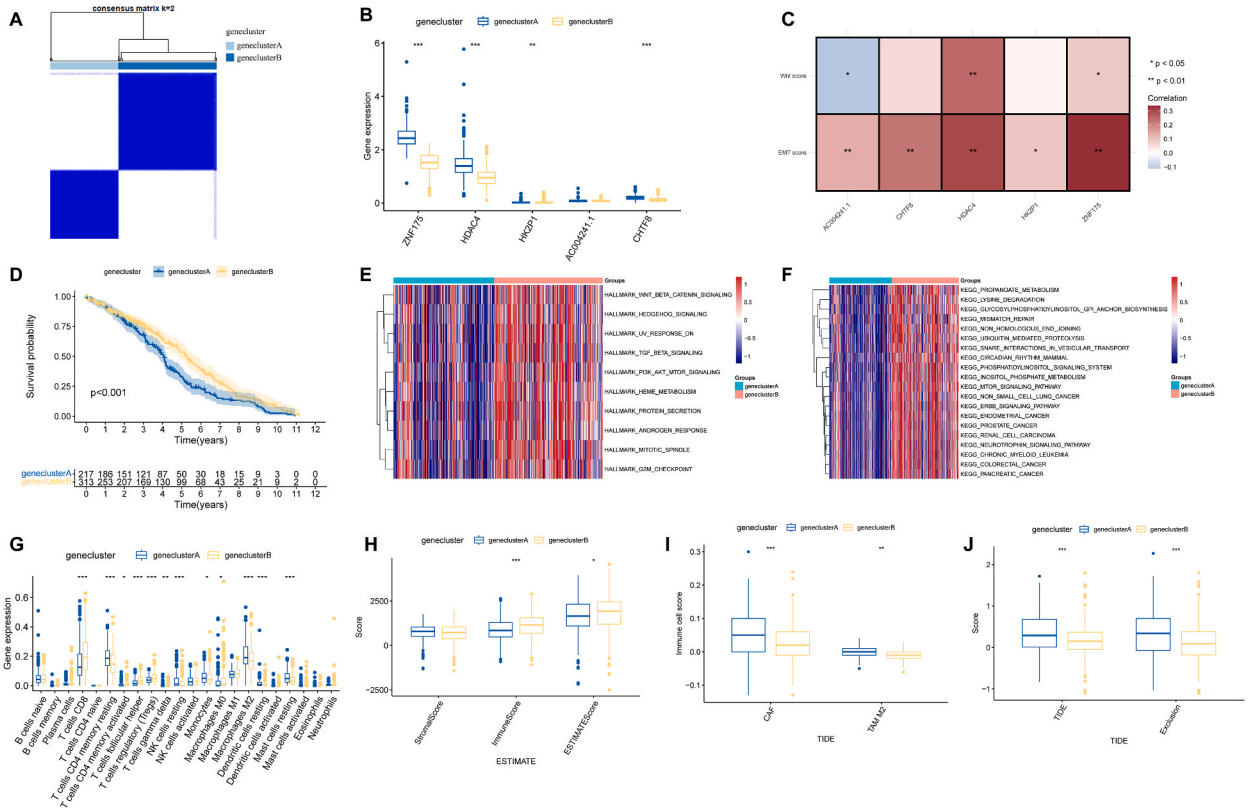

Fig. 6. Differences in TIME between clusters. (A) Two geneclusters were identified based on the five key DEGs by unsupervised clustering. (B) Differential expression of the five key DEGs between the geneclusters. (C) The correlation of five key DEGs with EMT and Wnt scores. (D) Kaplan–Meier survival analysis revealed the significant difference in survival between genecluster A and genecluster B. (E–F) The results of the HALLMARK and KEGG pathway scores. (G) The differences of immune cell infiltration between the different geneclusters. (H). The differences of Stromal score, Immune score, and ESTIMATE score between different geneclusters. (I–J) The differences in CAF, TAM M2, TIDE, and Exclusion scores between genecluster A and genecluster B.

M2, TIDE, and Exclusion in genecluster A than in genecluster B (Fig. 6I–J).

3.5. PCA score was established and the correlation between PCA score and immunotherapy

In this step, PCA analysis was conducted to score each ccRCC sample according to the PCA results and then divided the ccRCC samples into HPSG and LPSG based on the PCA score (Fig. 7A–B) (Supplementary Table 8). Subsequently, we compared the PCA scores among cluster 1, cluster 2, and cluster 3, as well as between genecluster A and genecluster B. The results indicated that the PCA score in cluster 2 was the highest of the three clusters and PCA score in genecluster B was higher than that in genecluster A (Fig. 7C–D). Next, we further compared the prognostic differences between HPSG and LPSG through prognostic analysis. Our results demonstrated that the survival probability of patients in HPSG was higher than that of patients in LPSG ($P = 0.002$) (Fig. 7E). For 1-,5- and 8-year ccRCC survival, the AUCs of the PCA score were 0.652, 0.695, and 0.688, respectively (Fig. 7F). In addition, more infiltration of CD8 T cells, T cell follicular helper cells, Treg cells, and activated NK cells was detected in HPSG, whereas there was a more infiltration of CD4 memory resting T cells, M2 macrophages, and resting mast cells in LPSG compared with HPSG (Fig. 7G) (Supplementary Fig. 2F). Meanwhile, the expression levels of CTLA4, PDCD1, LAG3, and TIGIT in HPSG and LPSG were further compared between HPSG and LPSG and our results showed that the expression levels of CTLA4, PDCD1, LAG3, and TIGIT were higher in HPSG than in LPSG ($P < 0.01$) (Fig. 7H–K), suggesting that the ccRCC patients with a high PCA score may benefit more from immunotherapy.

Furthermore, we explored the abundance of immune cell infiltration in ccRCC samples with different TNM stages, and our results showed that mast cells, resting CD4 T cells, and NK cells were more abundant in low-grade and low-stage ccRCC samples, whereas the infiltration abundance of CD8 T cells, activated CD4 T cells, follicular helper T cells, and Treg cells was lower (Supplementary Fig. 3). NK cells and mast cells showed a gradual decreasing trend with the progression of T stage (Supplementary Fig. 3A). Infiltration levels of resting CD4 memory T cells decreased in ccRCC samples with lymphatic metastasis compared with ccRCC samples without lymph node metastasis (Supplementary Fig. 3C). In the ccRCC samples with distant metastasis, CD8 T cell infiltration levels were significantly elevated (Supplementary Fig. 3D). The infiltration levels of CD8 T cells, Tregs, and follicular helper T cells gradually increased with the

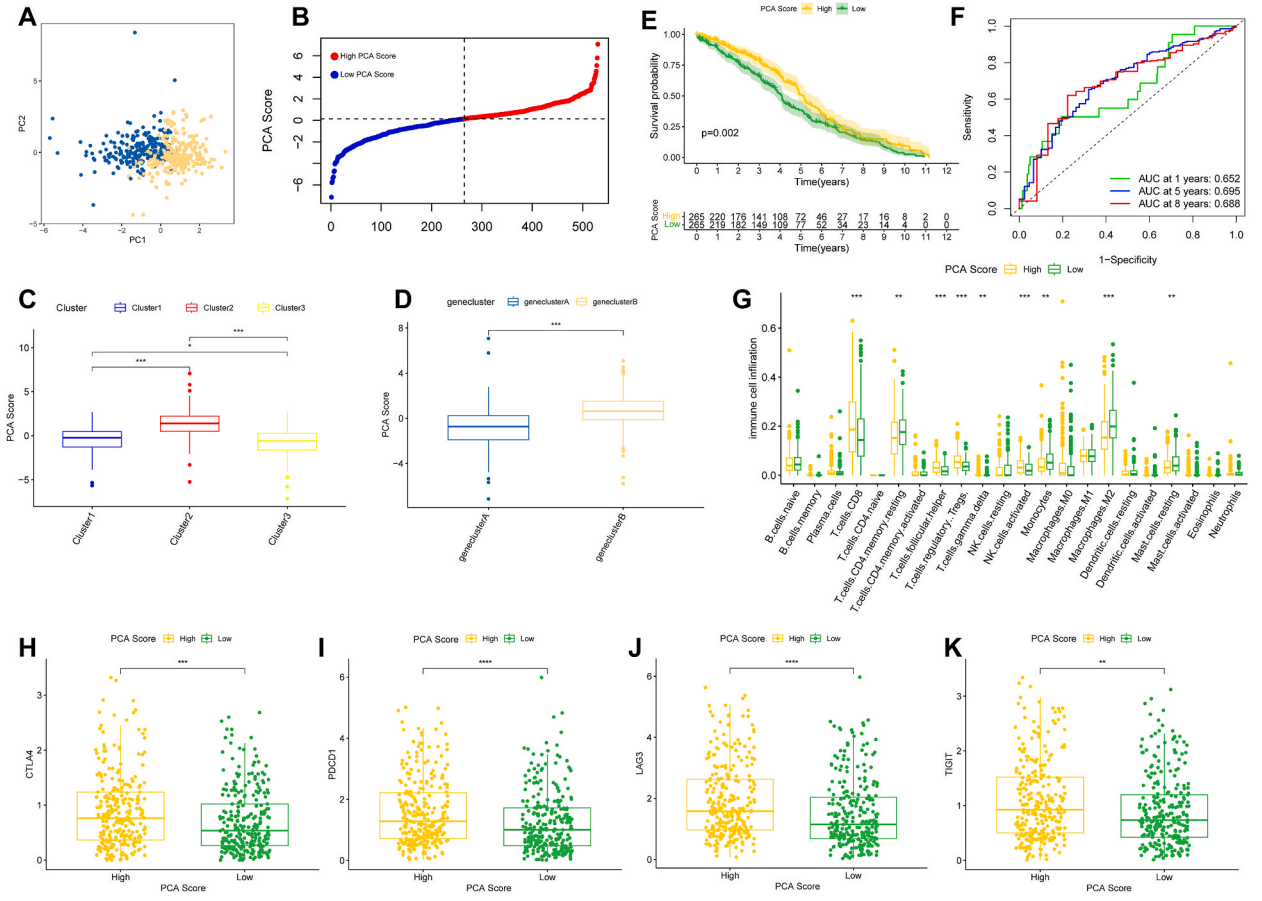

Fig. 7. Establishing a PCA Score. (A) The PCA diagram shows the distribution of the two geneclusters. (B) PCA score of each patient. (C–D) Differences in PCA score among three clusters and two geneclusters. (E) Kaplan–Meier survival analysis demonstrating a survival difference between HPSG and LPSG. (F) ROC curves analysis of PCA score. (G) The difference in the infiltration of immune cells between HPSG and LPSG. (H–K). Differential expression of immune checkpoints in HPSG and LPSG.

progression of stage, whereas the infiltration levels of M2 and mast cells gradually decreased with the progression of stage (Supplementary Figs. 3E–F). Meanwhile, by analyzing drug sensitivity at different TNM stages, we found that patients with low-grade or low-stage ccRCC showed more sensitivity to dalafenib (Supplementary Figs. 3G–J).

3.6. Correlation of PCA score with clinical features and drug sensitivity

Correlation between PCA score and multiple clinical characteristics in terms of survival status, age, stage, grade, and T stage was further conducted. Compared with patients in the alive group and the younger group (≤ 60), we found that patients in the death group and the older group (≥ 60) had higher PCA scores (Fig. 8A–B), suggesting that PCA score was correlated with patient survival and age. Meanwhile, PCA scores of patients with stage III/IV and T3/4 were higher than those of patients with stage I/II and T1/2 (Fig. 8C–D), indicating that PCA score correlated with the pathological status of ccRCC patients. In addition, we calculated the sensitivity of all ccRCC samples to 283 drugs (Supplementary Table 9). By comparing the drug sensitivity between the HPSG and LPSG, we found that patients in LPSG were more sensitive to targeted drugs (such as axitinib, dabrafenib, sunitinib, and temsirolimus) than patients in HPSG (Fig. 8E–H). Finally, the correlation between DRGs and PCA score were investigated, and the results showed that PCA score was positively correlated with NDUFA11, but negatively correlated with LRPPRC, NCKAP1, NDUSF1, and NUBPL, and there was no statistical difference in its correlation with other genes (Supplementary Fig. 2D). The correlation between the five key genes and PCA score showed that PCA score was positively correlated with AC004241.1, whereas negatively correlated with ZNF175, HDAC4, HK2P1, and CHTF8 (Supplementary Fig. 2D). Meanwhile, upon analyzing drug sensitivity at different TNM stages, we found that patients with low-grade or low-stage ccRCC were more sensitive to dalafenib (Supplementary Figs. 3G–J).

3.7. Immunohistochemical staining and experimental verification

In previous steps, we investigated the role of disulfidoptosis-related genes in ccRCC through bioinformatic approaches. In this step, to analyze the expression differences of the five key DEGs in ccRCC, we obtain and compared the immunohistochemical staining date from the HPA. The results showed that expression of HDAC4 and ZNF175 in tumor tissues were higher than normal tissues (Fig. 9A–B), with HDAC4 (Fig. 9A) predominantly expressed in the cytoplasm and nucleus, whereas ZNF175 (Fig. 9B) predominantly expressed in the cytoplasm. Immunohistochemical staining of the collected sections showed that HDAC4 was expressed in both tumors and normal tissues. However, its expression was markedly higher in the tumor tissue than that in the normal tissue (Fig. 9C). Next, the protein levels of HDAC4 in the ccRCC tissue and adjacent normal tissue were investigated through Western blotting, and our results confirmed that HDAC4 protein expression was higher in tumor tissues than in normal tissues (Fig. 9D). To gain an understanding of the role played by HDAC4 in ccRCC progression, we transfected 786-O cells with si-HDAC4 and si-NC, and our results showed that both protein

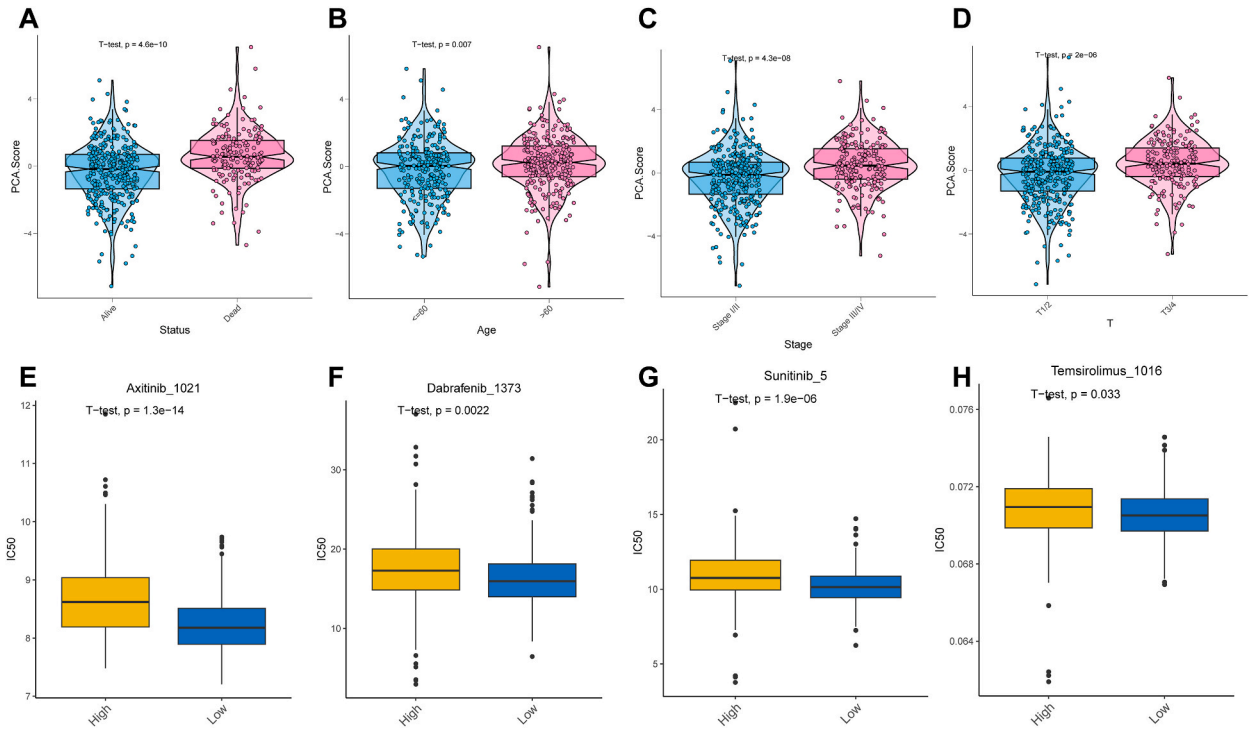

Fig. 8. Relationship between PCA score and clinical features and drug sensitivity. (A–D) The status, age, stage grade, and T stage were compared between HPSG and LPSG. (E–H) The box plot shows the sensitivities of HPSG and LPSG to Axitinib, Dabrafenib, Sunitinib and Temsirolimus.

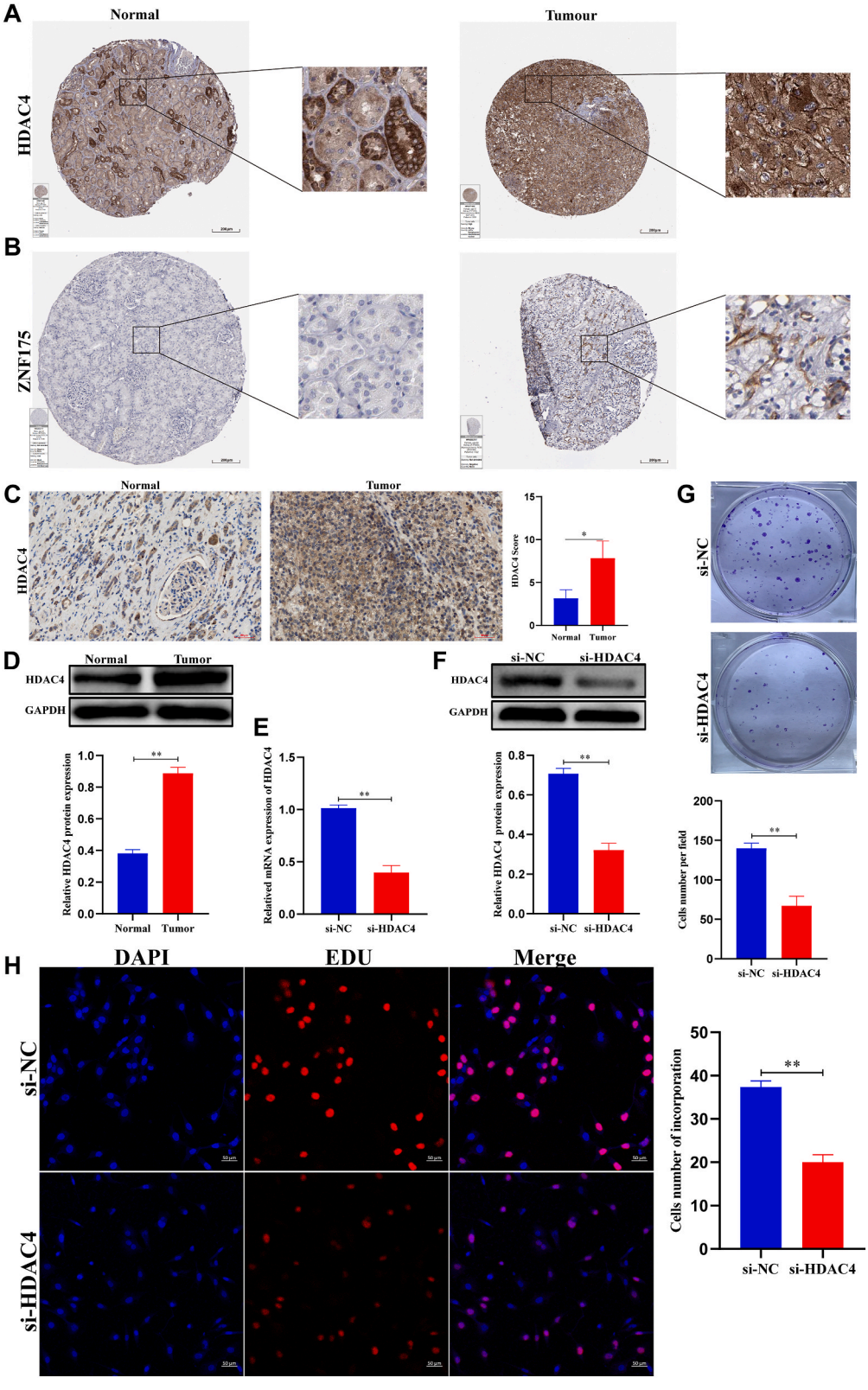

(caption on next page)

Fig. 9. Functional verification of HDAC4. (A–B) The differential expression of HDAC4 and ZNF175 between normal and tumor tissues from HPA database. (C) Immunohistochemical results of HDAC4 in paraffin sections of 30 patients with ccRCC. (D) Western blotting results showed differential expression of HDAC4 in 15 pairs of fresh ccRCC tissue (cancer and adjacent normal tissue). (E–F) Changes in HDAC4 protein and RNA levels in cells after HDAC4 knockdown. (G–H) Colony formation assay and EDU showed the changes in cell proliferation ability after knockdown of HDAC4. Note bene: an uncropped version of the original D–F is shown in Supplementary Figs. 4A–B.

and RNA levels of HDAC4 in si-HDAC4 group were lower than those in the si-NC group through Western blotting and qRT-PCR (Fig. 9E–F). In addition, results from the colony formation assay and EDU confirmed that the proliferative capacity of si-HDAC4 786-O cells was significantly lower than that of si-NC (Fig. 9G–H), suggesting that HDAC4 has the potential ability to promote cell proliferation and that HDAC4 plays a role in ccRCC progression.

3.8. *Diagram of the analysis mechanism of disulfidptosis in this study*

When glucose deprivation occurs, the abnormal disulfide bond formation of actin cytoskeleton proteins in slc7a11^{high} cells leads to actin network breakdown and disulfidptosis. The RAC1-WRC-mediated actin polymerization and lamellipodia formation may contribute to disulfidptosis through the formation of disulfide bonds between actin cytoskeletal proteins (Fig. 10).

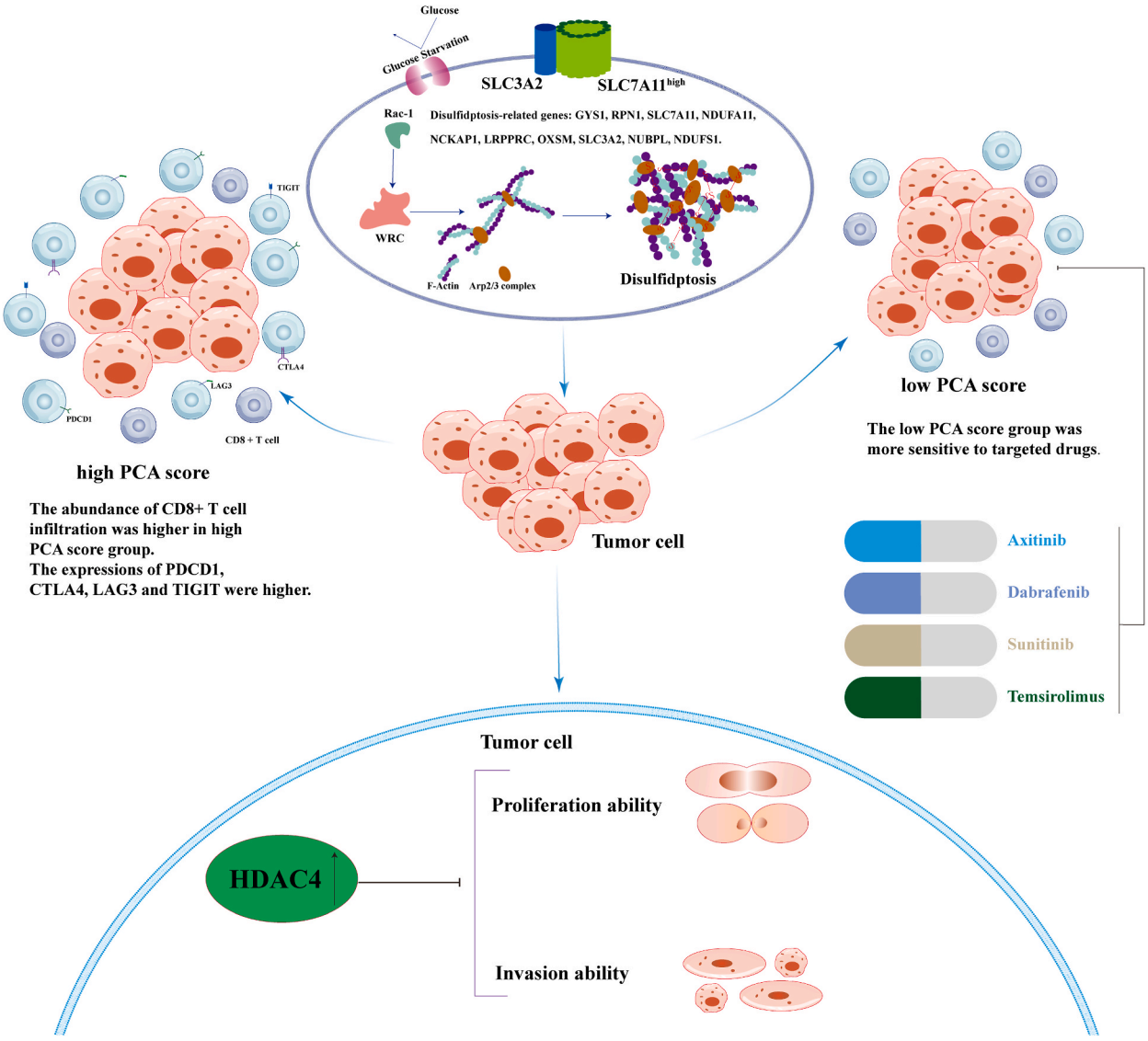

Fig. 10. Study mechanism diagram. Arp2/3: actin-related protein 2/3 complex; WRC: WAVE regulatory complex; F-actin: filamentous polymer of actin; Rac: a small G protein involved in actin polymerization and plate foot formation.

4. Discussion

ccRCC is the predominant RCC subtype, characterized by difficulties in early diagnosis. Localized ccRCC is mainly treated with surgery; however, there is no effective treatment for advanced and metastatic ccRCC because of its poor sensitivity to radiotherapy and chemotherapy. Fortunately, immunotherapy and targeted therapy bring hope to ccRCC patients [34]. However, because of the high heterogeneity of ccRCC, specific markers for the prognosis of the disease are lacking [35,36]. Therefore, finding effective ways or drugs to improve patient prognosis is crucial for patients with advanced ccRCC. Related studies have shown that other types of cell death such as pyroptosis, ferroptosis, and necroptosis greatly contributed to the progression of ccRCC [37]. Recently, disulfidptosis, a novel mode of apoptosis linked to the actin cytoskeleton, was discovered. Liu et al. found that when glucose was deficient in UMRC6 RCC cells with high SLC7A11 expression, the accumulation of disulfide bonds led to abnormal disulfide bond cross-linking between actin cytoskeletal proteins, ultimately leading to cell death [10]. Furthermore, inhibitors of glucose transporters GLUT1 and GLUT1/3 could suppress glucose uptake in cells, leading to the demise of cells with high SLC7A11 expression [10].

Disulfidptosis is closely related to tumor progression, and studies have found that disulfidptosis plays an important role in disease progression and prognosis in bladder, lung, breast, and cervical cancer [38–42]. Studies have confirmed that SLC7A11, SLC3A2, RPN1, NCKAP1, NDUFS1, NDUFA11, OXSM, NUBPL, and LRPPRC greatly contribute to the process of disulfidptosis, and interfering with these genes can effectively inhibit the progression of disulfidptosis. These genes were accordingly called DRGs. Some studies have found that mutations in DRGs may make a significant contribution to the occurrence and progression of tumors. Qi et al. found that 139 (22.56 %) of 616 lung adenocarcinoma samples had mutations associated with DRGs, with LRPPRC having the highest frequency of mutations [38]. However, Zhao et al. found that the incidence of DRG mutations was low in bladder cancer: only 16 out of 414 samples had mutations, and nonsense mutations were the main type, among which NCKAP1 mutation frequency was the highest (appearing in 12 samples) [39]. Furthermore, in a study on cervical cancer, the authors found that 32 out of 289 patients had mutations of DRGs, which were mainly nonsense mutations. Further, among all mutations, LRPPRC mutation had the highest rate of occurrence, observed in 10 samples [40]. In our study, similar to bladder cancer, we found that a low mutation rate of DRGs appeared in ccRCC, with 14 out of 530 samples showing mutations, and nonsense mutations were predominant. Among the genes, NDUFS1 had the highest mutation frequency. In addition, copy number loss of OXSM, NUBPL, RPN1, and SLC7A11 was dominant in ccRCC, whereas copy number amplification was dominant in NCKAP1, LRPPRC, and GYS1. NDUFS1 had the highest SNV percentage in ccRCC, followed by LRPPRC. Meanwhile, we found that LRPPRC, OXSM, and NUBPL in ccRCC samples had higher levels of methylation and the methylation level of NCKAP1 was positively correlated with mRNA expression. However, the methylation levels of NUBPL and NDUFA11 were negatively correlated with mRNA levels, indicating that the methylation of NCKAP1 led to an increase in its mRNA expression, whereas the methylation of NUBPL and NDUFA11 inhibited gene transcription, resulting in a decrease in mRNA level. We found that NCKAP1 and LRPPRC had the highest level of copy number heterozygote amplification, and OXSM had the highest level of copy number heterozygote deletion. Except for SLC7A11, CNV of the remaining genes was positively correlated with mRNA expression, where CNV level of NUBPL and RPN1 was strong positively correlated with mRNA expression. These results indicated that mutations of DRGs is not the main cause of ccRCC. However, for the 14 ccRCC patients with mutations of DRGs, the role of these mutations in the occurrence and progression of the disease needs to be further studied.

Current studies have demonstrated that disulfidptosis is closely associated with tumor progression and prognosis. In bladder cancer, Chen et al. constructed a prognostic model of DRGs by consistent cluster analysis and the results showed that the survival prognosis of bladder cancer patients with a high DRG score was significantly worse [41]. In breast cancer, four DEGs with prognostic value were selected based on DRGs, and a prognostic model was constructed. The results indicated that the overall survival of patients in the high score group was significantly worse than that of patients in the low score group [42]. In colorectal adenocarcinoma, Hu et al. selected 4 DRGs to construct a risk score model for predicting the survival and prognosis of patients, and the results showed that patients with high risk score had poor prognosis [43]. Our results suggested that ccRCC patients in HPSG have better prognosis than the patients in LPSG. Survival analyses of the 10 DRGs showed patients in the NUBPL high-expression group had significantly worse survival, and conversely, the survival prognosis of patients in the RPN1 high-expression group was better. This is inconsistent with the results reported in previous studies. This may be because of following factors: first, the tumor types were different; second, immunoinfiltrating CD8 T cells were more infiltrated in tumor tissues of patients in HPSG, and patients in HPSG were sensitive to immune checkpoint inhibitors, which may lead to prolonged survival of patients; third, patients in HPSG may have earlier tumor stages. These factors need to be further explored in future studies.

In our study, five key DEGs were identified for further study through univariate, multivariate, and LASSO regression analyses. These included histone deacetylase 4 (HDAC4), zinc finger protein 175 (ZNF175), chromosome transmission fidelity factor 8 (CHTF8), AC004241.1, and hexokinase 2 pseudogene 1 (HK2P1). ZNF175 contains 13 zinc finger structures and acts as a transcriptional repressor that reduces viral replication capacity and inhibits the expression of some chemokines [44]. HDAC4 is located in the nucleus and cytoplasm [45]. It plays a role in the progression of some tumors and has the potential to become a therapeutic target. In nasopharyngeal carcinoma, HDAC4 promotes EMT by inhibiting the transcription of E-cadherin [45]. In a study on ovarian cancer, patients with high HDAC4 expression were associated with poor overall survival and progression-free survival [46]. Consistent with the results reported in the literature, in our study, survival analysis showed that patients with high expression levels of HDAC4, ZNF175, CHTF8, and AC004241.1 had worse survival outcomes than those with low expression levels, implying their role as risk genes in ccRCC. Furthermore, immunohistochemical results of HDAC4 and ZNF175 from the HPA database showed that the expression of HDAC4 and ZNF175 was higher in tumor tissues. CHTF8 encodes the short protein that forms the Ctf18-RFC complex and is responsible for maintaining the stability of the complex [47]. Our results showed that patients with high CHTF8 expression in ccRCC had worse survival than those with low expression. The Wnt signaling pathway is a complex network of proteins that plays a role in embryonic

development and tumor progression, and aberrant activation of the Wnt signaling pathway promotes tumor cell growth and metastasis in colorectal, ovarian, breast, and other cancers [48]. EMT is key to tumor cell metastasis, and in breast cancer, the progression and metastasis can be controlled by inhibiting the progression of EMT [49,50]. Our results showed that five key DEGs were all positively correlated with the EMT score, whereas HDAC4 and ZNF175 had a strong positive correlation with the Wnt score, suggesting that the expression of the five key DEGs, especially HDAC4 and ZNF17, was closely associated with tumor progression. Furthermore, using PCA score of five key DEGs to divide the ccRCC samples into HPSG and LPSG, and survival analyses showed that patients in LPSG had a significantly worse survival prognosis. Similarly, the clinical information results showed that patients in HPSG were associated with a higher proportion of deaths. Furthermore, a higher proportion of patients in HPSG were at stage III/IV and T3/4 compared with the proportion of patients in LPSG. Drug sensitivity analyses showed that patients in LPSG were more sensitive to four commonly targeted drugs. Finally, the function of the key gene HDAC4 in ccRCC was experimentally verified. The experiments confirmed that the protein level of HDAC4 was much higher in cancerous tissues than in healthy tissues, and also verified that HDAC4 has the ability to promote the proliferation of cancer cells.

Tumor mircroenviroment (TME) mainly comprises tumor cells, immune cells, and cytokines, which are the survival environment for tumor cells and play a supportive role in tumor progression [51]. Of these, CD8 T cells are a crucial element in contemporary tumor immunotherapy [52]. For example, in triple-negative breast cancer (TNBC), a high abundance of $CD8^+$ T cells in the tumor tissue is associated with a good prognosis [53]. However, most studies have shown that immune escape of tumor cells can be induced by reducing or inhibiting the infiltration of $CD8^+$ T cells. Tregs are another subset of $CD4^+$ T cells, the main function of which is to regulate immune responses [54]. Treg cells have a complex role in immunity, which includes maintaining the stability of the immune microenvironment by suppressing excessive immune responses. In pancreatic cancer, the infiltration extent of Treg cells is correlated with the pathological changes, grade, and stage of the tumor. When the degree of Treg cell infiltration increases, it often indicates a poor prognosis of pancreatic cancer patients [55]. Similarly, in patients with TNBC, the upregulation of Treg cells in tumor tissues is associated with poor prognosis [56]. TAMs are one of the most abundant immune cells in the TME [57]. M2 cells play an important role in tumor progression and metastasis, and are also associated with poor prognosis of patients [58]. Mononuclear cells could differentiate into M2 cells when stimulated with IL-4 [59]. In contrast, a large number of M2 cells infiltrated in the TME are associated with drug resistance and poor prognosis [60]. In lung cancer, large numbers of infiltrating M2 cells can assist in tumor metastasis by promoting EMT, but when the number of M2 cells is reduced, tumor growth is inhibited and immunotherapy and chemotherapy are more effective [61]. Our results suggested that PCA scores were positively correlated with $CD8^+$ T cells and T follicular helper cells, but negatively correlated with M2 cells. Furthermore, higher $CD8^+$ T cell infiltration and higher expression of four common immune checkpoints were detected in HPSG, suggesting that patients in HPSG may be more responsive to immunotherapy. Meanwhile, patients in HPSG had a better prognosis than those in LPSG.

Usually, ccRCC is not sensitive to radiotherapy and chemotherapy. However, immunotherapy and targeted therapies have made great progress and achieved good results in RCC, and have become important options for RCC treatment. CTLA4 is a transmembrane protein present on NK cells and activated T cells, which mainly acts by competitive binding to B7-1 and B7-2 ligands. Therefore, blocking the binding of CTLA4 to its ligands can abolish the suppressed state of T cell activity and reactivate the immune response of T cells. CTLA4 inhibitors can also negatively regulate Treg cells by targeting macrophages to improve the killing ability of immune cells against tumors [62]. This indicates the potential to inhibit tumor growth by targeting CTLA4. PDCD1 encodes a cell surface membrane protein, which is mainly expressed in B cells, natural killer T cells, CD4+/CD8+ T cells, and activated monocytes [63]. High PDCD1 expression is associated with poor survival in ccRCC [64]. LAG3 mainly exists on the surface of tumor infiltrating lymphocytes and can promote the immune escape of tumor cells by interacting with tumor cells [65]. Its inhibitors have achieved some success in the treatment of gastric cancer, non-small cell lung cancer, and breast cancer [66–68]. TIGIT is mainly expressed in effector T cells, Treg cells, memory T cells, and NK cells [69]. Further, several studies have shown that TIGIT is expressed to varying degrees in colon adenocarcinoma, endometrioid carcinoma, breast cancer, and ccRCC [70]. In ovarian cancer, the NK cell response to cancer cells was enhanced by blocking TIGIT, suggesting that targeting TIGIT is a potential immunotherapy to enhance the prognosis of ovarian cancer [71]. In our study, we found that the expression of four immune checkpoints in HPSG was higher than that in LPSG. Interestingly, through drug sensitivity analysis, we found that the patients in LPSG were more sensitive to axitinib, sunitinib, dabrafenib, and temsirolimus than those in HPSG. In summary, the HPSG showed a better response to immune checkpoint blockade therapy, whereas the LPSG was more sensitive to targeted drug therapy. Therefore, for the treatment of ccRCC, we could guide patients to use drugs according to the patients' PCA score of disulfidptosis key DEGs. For patients with a high PCA score, immunotherapy can be initiated according to our study results, which may improve the patient prognosis. For patients with low PCA score, we can choose mainly targeted therapy and strengthen follow-up to prolong patient survival. However, we must be aware that such exploration must be gradual and requires long, large number sample attempts.

In this study, through in-depth analysis of disulfidptosis and related genes in ccRCC, the contributions of DRGs in the diagnosis and treatment of ccRCC was found. However, we must also clearly recognize the shortcomings in our work. First, the data used in this study were obtained from public databases, which may suffer from data bias and insufficient sample size. Second, the results of this study need to be validated in different cohorts and large samples. Finally, this study only verified the functional role of the genes at the cellular level, and the results need to be further verified by in vivo experiments.

In conclusion, the study of disulfidptosis, as a new cell death type, can improve our understanding of the apoptosis mode of tumor cells. Our results revealed the high predictive value of genetic models based on DRGs in the prognosis and treatment of patients with ccRCC, and our findings have been validated by HDAC4 in RCC. In the future, we can use the gene model of disulfidptosis to guide the preoperative diagnosis, postoperative prediction, and drug treatment of advanced ccRCC patients. Moreover, based on the key genes, further studies may transform these genes into new tumor markers for RCC diagnosis and prognosis. For example, HDAC4, which was

associated with immune infiltration, was predictive of immunotherapy efficacy and may be a potential new molecular target for RCC treatment. However, these need to be confirmed by large sample trials and clinical studies, and the detailed mechanism of action of HDAC4 in ccRCC also needs to be further clarified by in vivo experiments.

Ethics approval and consent to participate

The study protocol was approved by the Ethics Committee of the First Affiliated Hospital of Henan University of Science and Technology.

Funding statement

This work was supported by the Medical Science and Technology project of Henan Province (No.LHGJ20200582) and (No. LHGJ20230460).

Data availability statement

Sharing research data helps other researchers evaluate your findings, build on your work and to increase trust in your article. We encourage all our authors to make as much of their data publicly available as reasonably possible. Please note that your response to the following questions regarding the public data availability and the reasons for potentially not making data available will be available alongside your article upon publication.

CRediT authorship contribution statement

Shiyong Xin: Writing – review & editing, Writing – original draft, Supervision, Resources, Project administration, Funding acquisition, Data curation, Conceptualization. **Junjie Su:** Writing – original draft, Visualization, Validation, Software. **Ruixin Li:** Visualization, Validation, Software. **Qiong Cao:** Validation. **Haojie Wang:** Validation. **Zhihao Wei:** Validation. **Chengliang Wang:** Investigation. **Chengdong Zhang:** Resources. **Jianguo Zhang:** Supervision. **Zheng Zhang:** Data curation. **Guanyu Li:** Methodology. **Wang Qin:** Data curation.

Declaration of competing interest

The authors declare that they have no known competing financial interests or personal relationships that could have appeared to influence the work reported in this paper.

Acknowledgement

We would like to express our gratitude to Qiong Cao and Zhihao Wei for their invaluable assistance during the experimental validation. We are particularly grateful to the MogoEdit (http://www.mogoedit.com/login) for the language polishing.

Appendix A. Supplementary data

Supplementary data to this article can be found online at https://doi.org/10.1016/j.heliyon.2024.e32258.

References

[1] J.J. Hsieh, M.P. Purdue, S. Signoretti, et al., Renal cell carcinoma, Nat. Rev. Dis. Prim. 3 (2017) 17009, https://doi.org/10.1038/nrdp.2017.9. Published 2017 Mar 9.
[2] T. Jiang, X. Diao, M. Ding, et al., SR-B1 and CD10 combined immunoprofile for differential diagnosis of metastatic clear cell renal cell carcinoma and clear cell carcinoma of the ovary, J. Mol. Histol. 52 (3) (2021) 539–544, https://doi.org/10.1007/s10735-021-09963-3.
[3] B.I. Rini, S.C. Campbell, B. Escudier, Renal cell carcinoma, Lancet 373 (9669) (2009) 1119–1132, https://doi.org/10.1016/S0140-6736(09)60229-4.
[4] M.B. Atkins, N.M. Tannir, Current and emerging therapies for first-line treatment of metastatic clear cell renal cell carcinoma, Cancer Treat Rev. 70 (2018) 127–137, https://doi.org/10.1016/j.ctrv.2018.07.009.
[5] E. Koren, Y. Fuchs, Modes of regulated cell death in cancer, Cancer Discov. 11 (2) (2021) 245–265, https://doi.org/10.1158/2159-8290.CD-20-0789.
[6] D. Tang, R. Kang, T.V. Berghe, P. Vandenabeele, G. Kroemer, The molecular machinery of regulated cell death, Cell Res. 29 (5) (2019) 347–364, https://doi.org/10.1038/s41422-019-0164-5.
[7] X. Jiang, B.R. Stockwell, M. Conrad, Ferroptosis: mechanisms, biology and role in disease, Nat. Rev. Mol. Cell Biol. 22 (4) (2021) 266–282, https://doi.org/10.1038/s41580-020-00324-8.
[8] J. Wang, D. Qin, Z. Tao, et al., Identification of cuproptosis-related subtypes, construction of a prognosis model, and tumor microenvironment landscape in gastric cancer, Front. Immunol. 13 (2022) 1056932, https://doi.org/10.3389/fimmu.2022.1056932. Published 2022 Nov 21.
[9] Z. Bian, R. Fan, L. Xie, A novel cuproptosis-related prognostic gene signature and validation of differential expression in clear cell renal cell carcinoma, Genes 13 (5) (2022) 851, https://doi.org/10.3390/genes13050851. Published 2022 May 10.
[10] X. Liu, L. Nie, Y. Zhang, et al., Actin cytoskeleton vulnerability to disulfide stress mediates disulfidptosis, Nat. Cell Biol. 25 (3) (2023) 404–414, https://doi.org/10.1038/s41556-023-01091-2.

[11] P. Koppula, L. Zhuang, B. Gan, Cystine transporter SLC7A11/xCT in cancer: ferroptosis, nutrient dependency, and cancer therapy, Protein Cell 12 (8) (2021) 599–620, https://doi.org/10.1007/s13238-020-00789-5.
[12] X.X. Liu, X.J. Li, B. Zhang, et al., MicroRNA-26b is underexpressed in human breast cancer and induces cell apoptosis by targeting SLC7A11, FEBS Lett. 585 (9) (2011) 1363–1367, https://doi.org/10.1016/j.febslet.2011.04.018.
[13] W. Guo, Y. Zhao, Z. Zhang, et al., Disruption of xCT inhibits cell growth via the ROS/autophagy pathway in hepatocellular carcinoma, Cancer Lett. 312 (1) (2011) 55–61, https://doi.org/10.1016/j.canlet.2011.07.024.
[14] G.W. Prager, M. Poettler, M. Schmidinger, et al., CD98hc (SLC3A2), a novel marker in renal cell cancer, Eur. J. Clin. Invest. 39 (4) (2009) 304–310, https://doi.org/10.1111/j.1365-2362.2009.02096.x.
[15] M. Poettler, M. Unseld, K. Braemswig, A. Haitel, C.C. Zielinski, G.W. Prager, CD98hc (SLC3A2) drives integrin-dependent renal cancer cell behavior, Mol. Cancer 12 (2013) 169, https://doi.org/10.1186/1476-4598-12-169. Published 2013 Dec 21.
[16] W.J. Shen, Y. Zhang, RPN1 promotes the proliferation and invasion of breast cancer cells by activating the PI3K/AKT/mTOR signaling pathway, Discov Oncol 15 (1) (2024) 25, https://doi.org/10.1007/s12672-024-00875-8. Published 2024 Feb 1.
[17] J. Lu, S.L. Wang, Y.C. Wang, et al., High WAVE3 expression correlates with proliferation, migration and invasion in human ovarian cancer, Oncotarget 8 (25) (2017) 41189–41201, https://doi.org/10.18632/oncotarget.17141.
[18] S.L. Chen, Q.S. Huang, Y.H. Huang, et al., GYS1 induces glycogen accumulation and promotes tumor progression via the NF-κB pathway in Clear Cell Renal Carcinoma, Theranostics 10 (20) (2020) 9186–9199, https://doi.org/10.7150/thno.46825. Published 2020 Jul 14.
[19] J. Ellinger, M. Poss, M. Brüggemann, et al., Systematic expression analysis of mitochondrial complex I Identifies NDUFS1 as a Biomarker in clear-cell renal-cell carcinoma, Clin. Genitourin. Cancer 15 (4) (2017) e551–e562, https://doi.org/10.1016/j.clgc.2016.11.010.
[20] W. Mao, G. Xiong, Y. Wu, et al., RORα suppresses cancer-associated Inflammation by repressing Respiratory complex I-dependent ROS generation, Int. J. Mol. Sci. 22 (19) (2021) 10665, https://doi.org/10.3390/ijms221910665. Published 2021 Oct 1.
[21] Y. Wang, N. Wu, D. Sun, et al., NUBPL, a novel metastasis-related gene, promotes colorectal carcinoma cell motility by inducing epithelial-mesenchymal transition, Cancer Sci. 108 (6) (2017) 1169–1176, https://doi.org/10.1111/cas.13243.
[22] H.Y. Zhang, Y.D. Ma, Y. Zhang, J. Cui, Z.M. Wang, Elevated levels of autophagy-related marker ULK1 and mitochondrion-associated autophagy inhibitor LRPPRC are associated with biochemical progression and overall survival after androgen deprivation therapy in patients with metastatic prostate cancer, J. Clin. Pathol. 70 (5) (2017) 383–389, https://doi.org/10.1136/jclinpath-2016-203926.
[23] X. Li, L. Lv, J. Zheng, et al., The significance of LRPPRC overexpression in gastric cancer, Med. Oncol. 31 (2) (2014) 818, https://doi.org/10.1007/s12032-013-0818-y.
[24] W.S. Wei, N. Wang, M.H. Deng, et al., LRPPRC regulates redox homeostasis via the circANKHD1/FOXM1 axis to enhance bladder urothelial carcinoma tumorigenesis, Redox Biol. (2021), https://doi.org/10.1016/j.redox.2021.102201. Published online November 27.
[25] G. Hu, H. Yao, Z. Wei, et al., A bioinformatics approach to identify a disulfidptosis-related gene signature for prognostic implication in colon adenocarcinoma, Sci. Rep. 13 (1) (2023) 12403, https://doi.org/10.1038/s41598-023-39563-y. Published 2023 Jul 31.
[26] M.E. Ritchie, B. Phipson, D. Wu, et al., Limma powers differential expression analyses for RNA-sequencing and microarray studies, Nucleic Acids Res. 43 (7) (2015) e47, https://doi.org/10.1093/nar/gkv007.
[27] M.D. Wilkerson, D.N. Hayes, ConsensusClusterPlus: a class discovery tool with confidence assessments and item tracking, Bioinformatics 26 (12) (2010) 1572–1573, https://doi.org/10.1093/bioinformatics/btq170.
[28] S. Hänzelmann, R. Castelo, J. Guinney, GSVA: gene set variation analysis for microarray and RNA-seq data, BMC Bioinf. 14 (2013) 7, https://doi.org/10.1186/1471-2105-14-7. Published 2013 Jan 16.
[29] D. Hanahan, Hallmarks of cancer: new dimensions, Cancer Discov. 12 (1) (2022) 31–46, https://doi.org/10.1158/2159-8290.CD-21-1059.
[30] K. Yoshihara, M. Shahmoradgoli, E. Martínez, et al., Inferring tumour purity and stromal and immune cell admixture from expression data, Nat. Commun. 4 (2013) 2612, https://doi.org/10.1038/ncomms3612.
[31] P. Jiang, S. Gu, D. Pan, et al., Signatures of T cell dysfunction and exclusion predict cancer immunotherapy response, Nat. Med. 24 (10) (2018) 1550–1558, https://doi.org/10.1038/s41591-018-0136-1.
[32] D. Maeser, R.F. Gruener, R.S. Huang, oncoPredict: an R package for predicting in vivo or cancer patient drug response and biomarkers from cell line screening data, Briefings Bioinf. 22 (6) (2021) bbab260, https://doi.org/10.1093/bib/bbab260.
[33] M. Uhlen, C. Zhang, S. Lee, et al., A pathology atlas of the human cancer transcriptome, Science 357 (6352) (2017) eaan2507, https://doi.org/10.1126/science.aan2507.
[34] V.J. Chen, G. Hernandez-Meza, P. Agrawal, et al., Time on therapy for at Least three Months correlates with overall survival in metastatic renal cell carcinoma, Cancers 11 (7) (2019) 1000, https://doi.org/10.3390/cancers11071000. Published 2019 Jul 17.
[35] J.I. López, Intratumor heterogeneity in clear cell renal cell carcinoma: a review for the practicing pathologist, APMIS 124 (3) (2016) 153–159, https://doi.org/10.1111/apm.12500.
[36] A.T. Beksac, D.J. Paulucci, K.A. Blum, S.S. Yadav, J.P. Sfakianos, K.K. Badani, Heterogeneity in renal cell carcinoma, Urol. Oncol. 35 (8) (2017) 507–515, https://doi.org/10.1016/j.urolonc.2017.05.006.
[37] X. Peng, J. Zhu, S. Liu, et al., Signature construction and molecular subtype identification based on cuproptosis-related genes to predict the prognosis and immune activity of patients with hepatocellular carcinoma, Front. Immunol. 13 (2022) 990790, https://doi.org/10.3389/fimmu.2022.990790. Published 2022 Sep. 28.
[38] C. Qi, J. Ma, J. Sun, X. Wu, J. Ding, The role of molecular subtypes and immune infiltration characteristics based on disulfidptosis-associated genes in lung adenocarcinoma, Aging 15 (11) (2023) 5075–5095, https://doi.org/10.18632/aging.204782.
[39] S. Zhao, L. Wang, W. Ding, et al., Crosstalk of disulfidptosis-related subtypes, establishment of a prognostic signature and immune infiltration characteristics in bladder cancer based on a machine learning survival framework, Front. Endocrinol. 14 (2023) 1180404, https://doi.org/10.3389/fendo.2023.1180404. Published 2023 Apr 19.
[40] L. Liu, J. Liu, Q. Lyu, et al., Disulfidptosis-associated LncRNAs index predicts prognosis and chemotherapy drugs sensitivity in cervical cancer, Sci. Rep. 13 (1) (2023) 12470, https://doi.org/10.1038/s41598-023-39669-3. Published 2023 Aug 1.
[41] H. Chen, W. Yang, Y. Li, L. Ma, Z. Ji, Leveraging a disulfidptosis-based signature to improve the survival and drug sensitivity of bladder cancer patients, Front. Immunol. 14 (2023) 1198878, https://doi.org/10.3389/fimmu.2023.1198878. Published 2023 May 30.
[42] Z. Wang, X. Du, W. Lian, et al., A novel disulfidptosis-associated expression pattern in breast cancer based on machine learning, Front. Genet. 14 (2023) 1193944, https://doi.org/10.3389/fgene.2023.1193944. Published 2023 Jun 29.
[43] G. Hu, H. Yao, Z. Wei, et al., A bioinformatics approach to identify a disulfidptosis-related gene signature for prognostic implication in colon adenocarcinoma, Sci. Rep. 13 (1) (2023) 12403, https://doi.org/10.1038/s41598-023-39563-y. Published 2023 Jul 31.
[44] J.J. Lu, D.Z. Lu, Y.F. Chen, et al., Proteomic analysis of hepatocellular carcinoma HepG2 cells treated with platycodin D, Chin. J. Nat. Med. 13 (9) (2015) 673–679, https://doi.org/10.1016/S1875-5364(15)30065-0.
[45] C. Huang, Z. Lin, X. Liu, et al., HDAC4 inhibitors as Antivascular Senescence therapeutics, Oxid. Med. Cell. Longev. 2022 (2022) 3087916, https://doi.org/10.1155/2022/3087916. Published 2022 Jun 29.
[46] X. Zhang, Z. Qi, H. Yin, G. Yang, Interaction between p53 and Ras signaling controls cisplatin resistance via HDAC4- and HIF-1α-mediated regulation of apoptosis and autophagy, Theranostics 9 (4) (2019) 1096–1114, https://doi.org/10.7150/thno.29673. Published 2019 Jan 30.
[47] T. Murakami, R. Takano, S. Takeo, et al., Stable interaction between the human proliferating cell nuclear antigen loader complex Ctf18-replication factor C (RFC) and DNA polymerase {epsilon} is mediated by the cohesion-specific subunits, Ctf18, Dcc1, and Ctf8, J. Biol. Chem. 285 (45) (2010) 34608–34615, https://doi.org/10.1074/jbc.M110.166710.
[48] J. Liu, Q. Xiao, J. Xiao, et al., Wnt/β-catenin signalling: function, biological mechanisms, and therapeutic opportunities, Signal Transduct. Targeted Ther. 7 (1) (2022) 3, https://doi.org/10.1038/s41392-021-00762-6. Published 2022 Jan 3.

[49] R. Gundamaraju, W. Lu, M.K. Paul, et al., Autophagy and EMT in cancer and metastasis: Who controls whom? Biochim. Biophys. Acta, Mol. Basis Dis. 1868 (9) (2022) 166431 https://doi.org/10.1016/j.bbadis.2022.166431.
[50] F. Bai, L.H. Zhang, X. Liu, et al., GATA3 functions downstream of BRCA1 to suppress EMT in breast cancer, Theranostics 11 (17) (2021) 8218–8233, https://doi.org/10.7150/thno.59280. Published 2021 Jul 13.
[51] M.T. Bilotta, A. Antignani, D.J. Fitzgerald, Managing the TME to improve the efficacy of cancer therapy, Front. Immunol. 13 (2022) 954992, https://doi.org/10.3389/fimmu.2022.954992. Published 2022 Oct 20.
[52] H. Raskov, A. Orhan, J.P. Christensen, I. Gögenur, Cytotoxic CD8+ T cells in cancer and cancer immunotherapy, Br. J. Cancer 124 (2) (2021) 359–367, https://doi.org/10.1038/s41416-020-01048-4.
[53] M. Oshi, M. Asaoka, Y. Tokumaru, et al., CD8 T cell score as a prognostic Biomarker for triple negative breast cancer, Int. J. Mol. Sci. 21 (18) (2020) 6968, https://doi.org/10.3390/ijms21186968. Published 2020 Sep. 22.
[54] J. Shimizu, S. Yamazaki, T. Takahashi, Y. Ishida, S. Sakaguchi, Stimulation of CD25(+)CD4(+) regulatory T cells through GITR breaks immunological self-tolerance, Nat. Immunol. 3 (2) (2002) 135–142, https://doi.org/10.1038/ni759.
[55] N. Hiraoka, K. Onozato, T. Kosuge, S. Hirohashi, Prevalence of FOXP3+ regulatory T cells increases during the progression of pancreatic ductal adenocarcinoma and its premalignant lesions, Clin. Cancer Res. 12 (18) (2006) 5423–5434, https://doi.org/10.1158/1078-0432.CCR-06-0369.
[56] G. Plitas, C. Konopacki, K. Wu, et al., Regulatory T cells Exhibit distinct features in human breast cancer, Immunity 45 (5) (2016) 1122–1134, https://doi.org/10.1016/j.immuni.2016.10.032.
[57] Y. Yan, J. Zhang, J.H. Li, et al., High tumor-associated macrophages infiltration is associated with poor prognosis and may contribute to the phenomenon of epithelial-mesenchymal transition in gastric cancer, OncoTargets Ther. 9 (2016) 3975–3983, https://doi.org/10.2147/OTT.S103112. Published 2016 Jun 30.
[58] M. Rakaee, L.R. Busund, S. Jamaly, et al., Prognostic value of macrophage Phenotypes in Resectable non-small cell lung cancer assessed by Multiplex immunohistochemistry, Neoplasia 21 (3) (2019) 282–293, https://doi.org/10.1016/j.neo.2019.01.005.
[59] P.J. Murray, J.E. Allen, S.K. Biswas, et al., Macrophage activation and polarization: nomenclature and experimental guidelines, Immunity 41 (1) (2014) 14–20, https://doi.org/10.1016/j.immuni.2014.06.008.
[60] S.D. Jayasingam, M. Citartan, T.H. Thang, A.A. Mat Zin, K.C. Ang, E.S. Ch'ng, Evaluating the polarization of tumor-associated macrophages into M1 and M2 phenotypes in human cancer tissue: technicalities and challenges in routine clinical practice, Front. Oncol. 9 (2020) 1512, https://doi.org/10.3389/fonc.2019.01512. Published 2020 Jan 24.
[61] J. Qin, X. Zhang, B. Tan, et al., Blocking P2X7-mediated macrophage polarization overcomes treatment resistance in lung cancer, Cancer Immunol. Res. 8 (11) (2020) 1426–1439, https://doi.org/10.1158/2326-6066.CIR-20-0123.
[62] T.R. Simpson, F. Li, W. Montalvo-Ortiz, et al., Fc-dependent depletion of tumor-infiltrating regulatory T cells co-defines the efficacy of anti-CTLA-4 therapy against melanoma, J. Exp. Med. 210 (9) (2013) 1695–1710, https://doi.org/10.1084/jem.20130579.
[63] Z. Li, N. Li, Q. Zhu, et al., Genetic variations of PD1 and TIM3 are differentially and interactively associated with the development of cirrhosis and HCC in patients with chronic HBV infection, Infect. Genet. Evol. 14 (2013) 240–246, https://doi.org/10.1016/j.meegid.2012.12.008.
[64] Y. Miao, J. Wang, Q. Li, et al., Prognostic value and immunological role of PDCD1 gene in pan-cancer, Int. Immunopharm. 89 (Pt B) (2020) 107080, https://doi.org/10.1016/j.intimp.2020.107080.
[65] C. Solinas, S. Garaud, P. De Silva, et al., Immune checkpoint molecules on tumor-infiltrating lymphocytes and their association with Tertiary lymphoid structures in human breast cancer, Front. Immunol. 8 (2017) 1412, https://doi.org/10.3389/fimmu.2017.01412. Published 2017 Oct 30.
[66] E.H. Jung, H.R. Jang, S.H. Kim, et al., Tumor LAG-3 and NY-ESO-1 expression predict durable clinical benefits of immune checkpoint inhibitors in advanced non-small cell lung cancer, Thorac Cancer 12 (5) (2021) 619–630, https://doi.org/10.1111/1759-7714.13834.
[67] K. Mimura, L.F. Kua, J.F. Xiao, et al., Combined inhibition of PD-1/PD-L1, Lag-3, and Tim-3 axes augments antitumor immunity in gastric cancer-T cell coculture models, Gastric Cancer 24 (3) (2021) 611–623, https://doi.org/10.1007/s10120-020-01151-8.
[68] E.S. Stovgaard, I. Kümler, K. List-Jensen, et al., Prognostic and Clinicopathologic Associations of LAG-3 expression in triple-negative breast cancer, Appl. Immunohistochem. Mol. Morphol. 30 (1) (2022) 62–71, https://doi.org/10.1097/PAI.0000000000000954.
[69] X. Yu, K. Harden, L.C. Gonzalez, et al., The surface protein TIGIT suppresses T cell activation by promoting the generation of mature immunoregulatory dendritic cells, Nat. Immunol. 10 (1) (2009) 48–57, https://doi.org/10.1038/ni.1674.
[70] X. Duan, J. Liu, J. Cui, et al., Expression of TIGIT/CD155 and correlations with clinical pathological features in human hepatocellular carcinoma, Mol. Med. Rep. 20 (4) (2019) 3773–3781, https://doi.org/10.3892/mmr.2019.10641.
[71] R.J. Maas, J.S. Hoogstad-van Evert, J.M. Van der Meer, et al., TIGIT blockade enhances functionality of peritoneal NK cells with altered expression of DNAM-1/TIGIT/CD96 checkpoint molecules in ovarian cancer, OncoImmunology 9 (1) (2020) 1843247, https://doi.org/10.1080/2162402X.2020.1843247. Published 2020 Nov 8.